UNIVERSITY OF TARTU

Faculty of Science and Technology

Institute of Physics

Laura Lõugas

USING RAPIDEYE HIGH SPATIAL RESOLUTION IMAGERY IN MAPPING SHALLOW COASTAL WATER BENTHIC HABITATS

Master thesis in Environmental technology (30 EAP)

Supervisor: Ph.D Tiit Kutser

Estonian Marine Institute, University of Tartu

Accepted for defense:

Supervisor:

Head of the department:

signature, date

Tartu 2015

Table of contents

Introduction

Nearly three-quarters of the Earth's surface is covered by oceans, seas and smaller inland water bodies. Large proportions of the human population, industry, agriculture, recreation and tourism are located near or in the coastal zones. Many benthic communities and ecosystems of coastal zones, estuaries and inland water bodies have both commercial and ecological value, which makes these regions valuable in terms of biodiversity and marine resources (Werdell & Roesler, 2003). In these areas we can find specific flora and fauna, but also it is a place where infrastructure develops and tourist facilities are located. The above mentioned anthropogenic factors are largely responsible for the deteriorating conditions of coastal waters. Therefore, it is necessary to plan carefully activities, which could affect the state of coastal waters and continuously monitor the conditions. Coastal zone receives all lands discharges, such as freshwater, erosion products and sewage, and it is highly affected by different marine processes, including wave action, tidal currents, as well as storm surges. Taking this into account one may conclude, that coastline is very valuable dynamical border area because its morphological and ecological characteristics (Barale & Folving, 1996).

Benthic habitats are important components of coastal zone ecosystem. The vegetation contributes to the primary production in coastal areas, supporting grazing and detrital food webs. Aquatic vegetation is also providing food, spawning and nursery grounds for fishes and other invertebrate species (Francour, 1997; Hemminga & Duarte, 2000). Benthic vegetation helps to prevent coastal erosion by binding sediments and reduces nutrient loading and other forms of pollution (Fonseca, 1989).

The health of vegetation communities in coastal waters depends on suitable environmental conditions. Submerged aquatic habitat requires light for photosynthesis, growth, and survival (Dennison, 1987). The minimal requirement for light conditions of a particular species determines the maximal water depth at which it can survive (Dennison et al. 1993). The eutrophication and nutrient enrichment of coastal waters is a result of human activities and is widely recognized as a world-wide pollution threat (Schramm & Nienhuis, 1996). Specific changes, such as decline or disappearance of certain plant communities, reduced diversity of the flora, blooms of short-lived annual forms and changes of depth distribution of benthic algae, have occurred in vegetation communities due to increasing eutrophication (Schramm & Nienhuis, 1996).

Sustainable management of coastal environments requires regular collection of accurate information on indicators of ecosystems health (Phinn et al., 2004). Benthic habitat cover and trends of the changes in it are indicators of water quality. The purpose of objective monitoring is to track short-term and long-term changes in species distribution and structure. Quantitative analysis of benthic habitats allows adequately assess the state of coastal marine environment, provide better evidence of environmental changes and describe the processes that are caused by human or nature activities. In addition, the benthic vegetation needs to be mapped for spatial planning of the seafloor use (for example wind parks and the construction of ports, conservation planning, regulation of fishing, etc.).

Various contact measurements provide accurate information about seafloor. Benthic habitat mapping by conventional methods (diving, underwater video, grab samples) provides good accuracy (Werdell & Roesler, 2003), but these are very expensive and limited by manpower and the time factor, which is necessary for mapping large areas. In addition, in some areas the weather could be a limitation for monitoring the seasonal changes by diving (Wittlinger & Zimmerman, 2000), or dangerous sea bottom can restrict the boat/ship from reaching the required area. Thus, the contact measurements do not ensure adequate and comprehensive information of the quantitative indicators of sea bottom and changes in it. Remote sensing methods significantly complement contact measurements and give additional information about the hard-to-reach areas. Remote sensing provides a potential opportunity to map the seabed rapidly and classify the benthic vegetation, because vegetation species differ in their optical properties. Time series of satellite imagery allow studying the long-term changes in benthic vegetation.

Mapping the types and biophysical properties of the substrate cover, based on their reflectance properties, has been carried out successfully in optically clear and shallow coastal waters like in coral reef areas (Anstee et al., 2000; Dekker et al., 2001; Kutser & Jupp, 2002; Phinn et al., 2004). Comparing with the reflectance properties of coral reef benthic habitats (Hochberg & Atkinson 2000, 2003; Karpouzli et al. 2004; Minghelli-Roman et al. 2002) and seagrass communities (Fyfe, 2003; Pasqualini et al. 2005), there is still not enough information about the reflectance properties of benthic algal species, especially of those growing in temperate waters. However, algal spectral reflectance properties have been published in some of the coral reef benthic community studies (Hochberg and Atkinson, 2000; Kutser et al., 2003). A few published reflectance spectra of various algal species are

presented in Maritorena et al. (1994), Wittlinger & Zimmerman (2000), Anstee et al. (2000), Kutser et al. (2006), Vahtmäe et al. (2006, 2011), Vahtmäe & Kutser (2013) and Kotta et al. (2014).

Most of the remote sensing benthic habitat mapping studies have been carried out in clear oceanic (Case I) waters. Case I waters were defined by Morel and Prieur (1977) as waters where the main optical properties are determined by phytoplankton. Suspended matter and coloured dissolved organic matter (CDOM) in these waters are predominantly products of decomposition of phytoplankton and their concentrations are in correlation with the amount of phytoplankton (commonly expressed as concentration of chlorophyll a). Therefore, to describe the optical properties of Case I waters only the concentration of chlorophyll a (as the main pigment of phytoplankton) is needed.

All of areas of interest are quite shallow coastal areas where most of the CDOM has terrestrial origin and therefore its concentration is not correlated with the concentration of phytoplankton. The same applies to suspended matter – it is mostly originated from nearby land or re-suspended from the sea bottom and is not phytoplankton degradation product.

Mapping seafloor of shallow near-shore areas has been carried out successfully with high spatial resolution satellite imagery like IKONOS (4 m resolution), QuickBird (2,4 m resolution) and WorldView-2 (2 m resolution) (Fornes et al., 2006; Mishra et al., 2006; Vahtmäe & Kutser, 2007; Ohlendorf et al., 2011; Tulldahl et al. 2013; Vahtmäe et al., 2011; Vahtmäe & Kutser, 2013). These images must be ordered before-hand and they typically cover area about 15x15 km. Therefore, mapping large areas and monitoring changes in benthic habitats, which needs long-time series, with the data of these satellites is relatively expensive and complicated. RapidEye constellation consist of 5 satellites, which pixel size is 5 meters and their global revisit time is only 1 day. This allows to get needed high resolution information frequently.

The main aim of this study was to determine whether RapidEye satellites are suitable for mapping benthic algal cover in shallow water coastal environment and with how much detail concerning different habitat types. The thesis provides also general principles of shallow water remote sensing, technical overview of the satellite, and the description of the processing methods used.

1 Aquatic remote sensing

Remote sensing is the science of getting information about an area, object or phenomenon through the analysis of data, which is acquired by a sensor that is not in physical contact with the area, object or phenomenon under investigation (Lillesand & Kiefer, 1999). Remote sensing data is recorded by a sensor, which measures the electromagnetic radiation or energy reflected from the object (Philipson, 2003). Remote sensing instruments are divided into active and passive. Active sensors provide their own energy source for illumination. The instrument emits radiation which is directed toward the target to be investigated. The radiation reflected from that target is detected and measured by the sensor. RADAR (RAdio Detection And Ranging) and LiDAR (Light Detection And Ranging) are examples of active remote sensing systems that can us provide information about the properties of the study object (Khoi & Munthali, 2012). Passive sensors gather natural radiation that is emitted or reflected by the object or surrounding areas. Reflected sunlight is the most common source of radiation and sensors using electromagnetic radiation emitted by the Sun are called passive sensors.

Water absorbs light very strongly in almost all wavelengths except the visible light region. For example, the radar rays are unable to penetrate the water deeper than few millimeters. Therefore, with remote sensing, information about the substances in the water and/or characteristics of benthic habitats, can be obtained using only visible light wavelengths (Bukata, 2005). LiDAR systems are very expensive and their study area is small, because the laser beam is narrow. These devices are usable only from airplanes or helicopters as otherwise the intensity of the laser beam required for the measurements becomes dangerous for living organisms. Low altitude means that even in the case of scanning instruments the swath is narrow. Also, the data is not continuous as certain time is needed to measure the laser beam backscattered from water and airplanes cover certain distance during this time period. All this means that the cost of unit of study area is very high if LIDAR sensors are used. Therefore, passive sensors are more suitable for mapping large areas and one of them is used in this study.

The radiance flux, which is measured above and below the water surface, consist of four different components (Figure 1): light that is backscattered from particles in the atmosphere (molecules of gases, solid particles); light reaching back to the sensor after reflection on the sea surface; light upwelling from the water column after backscattering in the water; light that is reflected off the bottom of the water body (provided that the water body is relatively

shallow and water sufficiently clear) (Sathyendranath, 2000). It must be noted that the part of the signal is absorbed in the process by gas molecules and absorbing aerosols in atmosphere, by optically active water constituents in the water column and different benthic habitats at the sea bottom.

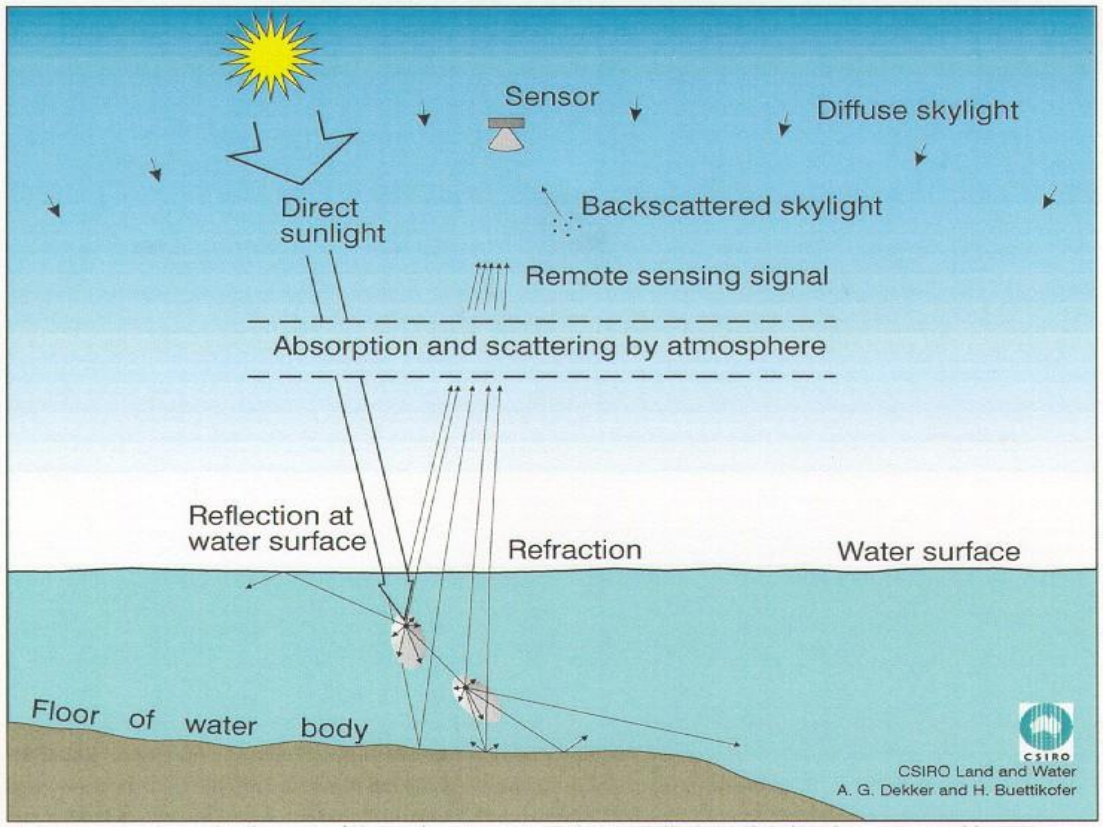

Figure 1. Components of the radiance flux measured by the remote sensing instruments.

In case of shallow water bodies, signal measured by remote sensing (the color of the water) is affected by the light which is backscattered from the bottom of the water body. This part of signal can give us information about the benthic habitats (IOCCG, 2000). The total signal reaching back to the sensor is highly affected by the atmosphere. In the case of satellite measurements above deep clear water the atmospheric contribution in the measured signal is more than 90%. This part of the measured signal does not give us any useful information about the sea surface, water column nor the seabed properties and needs to be removed from the signal (Bukata et al., 1995). The effects caused by atmosphere are eliminated with the atmospheric correction (IOCCG, 2010). Assumptions, made in atmospheric correction algorithms of offshore ocean areas (for example that there is no water leaving signal in near-infrared part of the spectrum due to strong absorption of radiation by water molecules), are not valid in shallow and/or turbid coastal areas and inland water bodies. In coastal waters also

the adjacency effect needs to be taken into account. Since water absorbs almost all of the radiation in most of the parts of the spectrum it looks nearly black from the space. Land, however, is relatively bright object. Light backscatters from the land into all directions and some of it scatters over water. Due to the big brightness difference of water and land, relatively large part of radiation measured above the near-shore water surface actually comes from the neighboring land.

Only fraction of the signal measured by a remote sensing sensor can provide us useful information about benthic habitats. Figure 1 illustrates the fate of sunlight while propagating through the atmosphere and water column and formation of the remote sensing signal. Only two of these four light fluxes contain information about the underwater light field and the composition of the aquatic medium, but only the last component gives the information about the type of benthic habitat. Rest of the three components are considered as noise that has to be removed when the interest is to map the benthic algal cover (Bukata et al., 1995).

1.1 Spectral properties of the seafloor

Spectral properties of the seafloor depend on benthic habitats covering it. Spectral data collected about optical properties of different benthic habitats (Maritorena et al., 1994; Wittlinger & Zimmerman, 2000; Anstee et al., 2000; Hochberg et al., 2003, 2004; Kutser et al., 2006; Vahtmäe et al., 2006, 2011; Vahtmäe & Kutser, 2013; Kotta et al., 2014) show that the main differences allowing to separate broad groups of algae (e.g. green, red and brown) from each other are in the red part of spectrum. For example red algae reflectance spectra have a distinct double peak at 600 nm and 650 nm, green algae and higher order plants have broad maxima around 550 nm and brown algae and corals (containing brown algae) reflectance have a peak around 610 as well as shoulders near 580 nm and 650 nm (Figures 2 and 3). These spectral features in red part of spectrum are too narrow to be detectable by multispectral instruments (Kutser et al., 2006b). The published data also suggest that it will not be possible to map benthic algal cover at species level unless the number of species is very small.

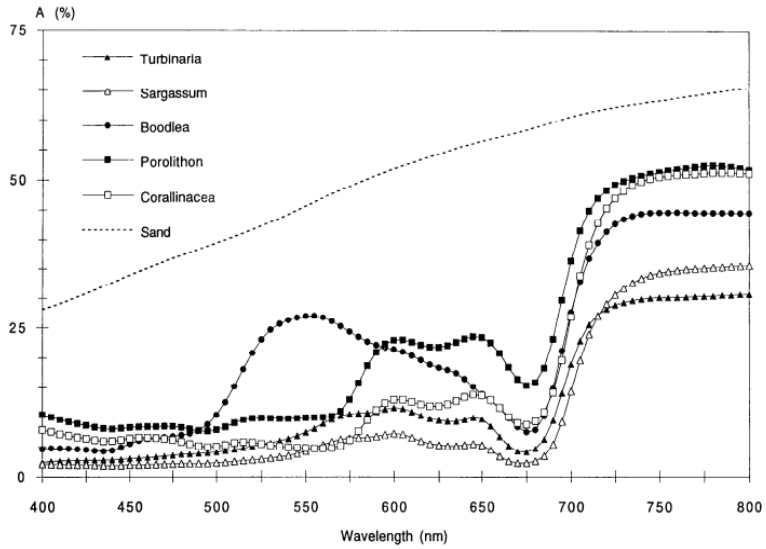

Figure 2. Spectral values of the albedo for various algae and coral sand (Maritorena et al., 1994).

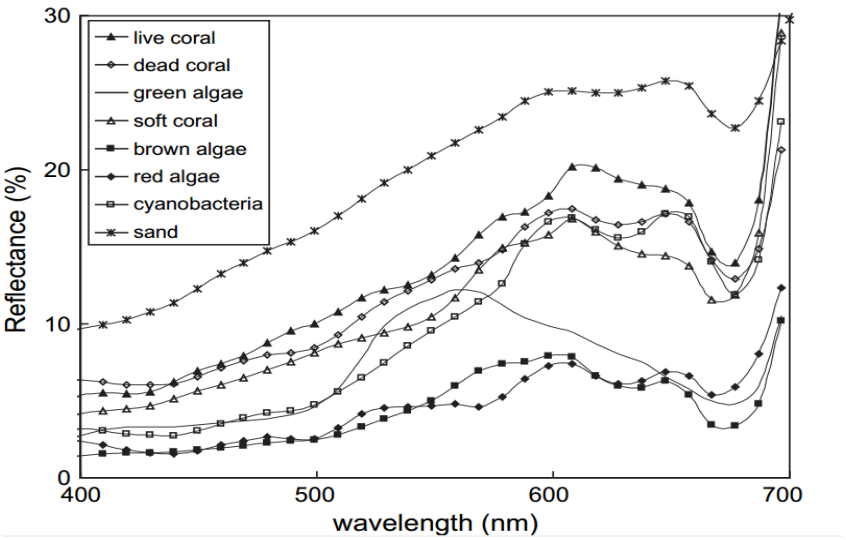

Figure 3. Radiance refletance spectra of different coral and algae species (Kutser et al., 2006a).

1.2 Optically active substances

Remote sensing signal is affected by the water itself alongside with optically active substances (OAS), which includes phytoplankton, colored dissolved organic matter (CDOM), and suspended solids. Optically active substances absorb or scatter light reaching into the water in their specific manner, forming the underwater light field and reflectance spectrum measured above the water surface.

Phytoplankton covers algal communities with various size distribution, which are dominating in the lit surface layer of the waters (Lalli & Parsons, 1994). The estimation of the amount of

phytoplankton is based on the concentration of photosynthetic pigment chlorophyll-a (Moses et al., 2009). The absorption spectrum of chlorophyll-a has two peaks located at wavelengths 440 nm and 675 nm (Laanen, 2007). Scattering properties of phytoplankton are variable. In most cases the scattering coefficient spectra of phytoplankton are relatively flat with slight decrease towards the longer wavelengths. However, cyanobacteria, containing gas vesicles, may have backscattering that is highly dependent on wavelength.

The concentration and type of dissolved organic matter (DOM) are treated as major water parameters, which indicate both natural and anthropogenic organic substances in the water. Optically active component of this matter is called colored dissolved organic matter (CDOM). During the decay of phytoplankton autochthonous (generated in the water body) CDOM is formed. In coastal and inland waters most of the CDOM has allochtonous origin. It is formed as soil degradation product and brought to the waterbodies by precipitation. CDOM absorbs light strongly in UV part of spectrum and the absorption is exponentially decreasing with increasing wavelength. Scattering properties of CDOM are usually considered negligible.

Total suspended matter (TSM) consist of light scattering organic and inorganic particles found in the water (IOCCG, 2000). In shallow coastal waters, suspended solids get into water from bottom sediments due to waves and currents, but also from land-based sources (sediment transport through rivers, erosion of the coast) where, as in open ocean, most of the suspended matter consist of detritus – degradation products of phytoplankton and zooplankton. Mineral suspended matter scatters more light than absorbs. Both, the scattering and absorption coefficients are relatively straight spectral functions (either completely independent of the wavelength or slightly decreasing with increasing wavelength) (Laanen, 2007). Phytoplankton degradation products have absorption properties similar to CDOM i.e. they absorb light strongly in UV part of spectrum and the absorption coefficient decreases exponentially with increasing wavelength.

1.3 Remote sensing of shallow waters

In shallow clear waters, where the water depth is much smaller than the potential for light to penetrate, fraction of the light beam may reach the bottom of the water body, be partly absorbed and be partly reflected from it. The spectrum of light emanating from the surface in shallow waters contains information of optical properties of the water and the benthic substrate (Werdell & Roesler, 2003). The light passing to benthos and reflecting from it, is

modified by spectral scattering and absorption by phytoplankton, suspended organic and inorganic matter and dissolved organic substances (Dekker et al., 1992). One of difficulties with remote sensing of benthic habitats is the confounding influence of variable depth on bottom reflectance (Mumby et al., 1998). It is hard to understand whether the reflectance spectrum changed due to changes in water depth or bottom type.

Calculations and measurements that examine the influence of water column depth indicate that the weakening of the flux in the water column is very fast (Wittlinger & Zimmermann, 2000). Light penetration depends on the wavelength and in oceanic waters it is greater in blue wavelengths (400 nm) than in red wavelengths (600 nm) (Mumby et al., 2003).

Depth of penetration (DOP) is described as the maximum depth, from where the light photons may come back to the water surface. The depth of penetration is inversely proportional to attenuation coefficient of water. Two examples of DOP spectra are shown in Figure 4.

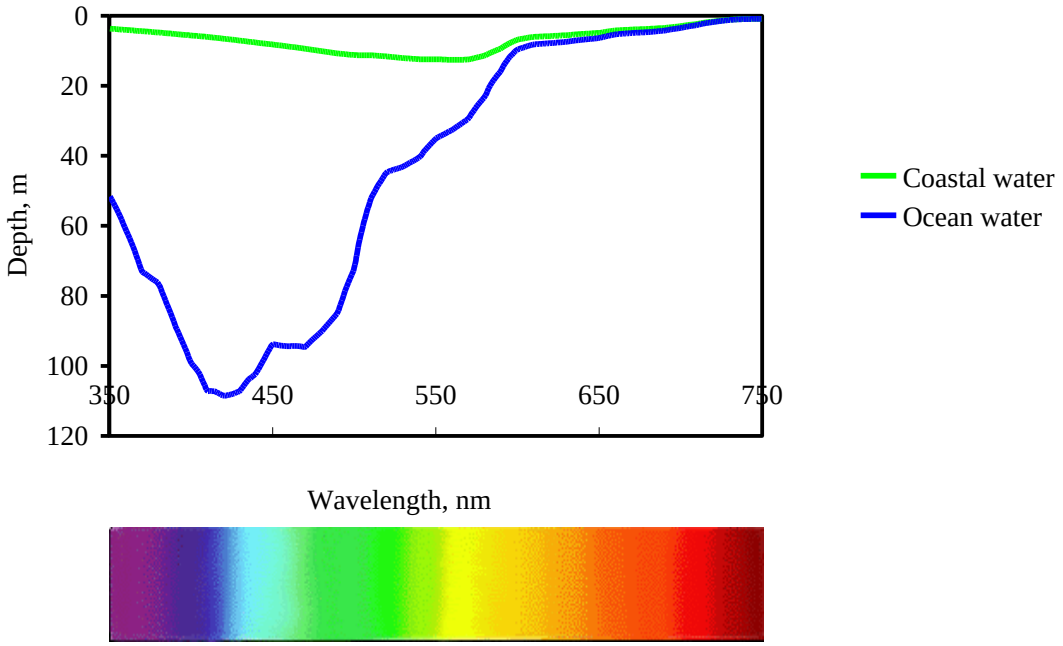

Figure 4. DOP spectra of coastal water and ocean water (Vahtmäe, 2005).

It is clearly seen in Figure 4 that at longer wavelengths the difference between depth of penetration in turbid coastal and clear oceanic water is small as the dominant factor affecting DOP at these wavelengths is absorption of light by water molecules that is identical in both cases. Smaller DOP in coastal waters at shorter wavelengths is the results of absorbing and

scattering properties of phytoplankton as well as light absorption by CDOM. The coastal water spectrum in Figure 4 represents the situation in the open parts of the Baltic Sea.

Altogether, mapping benthic habitats with remote sensing method is complicated due to water column properties, varying water depth and the complex mosaics of bottom types. Increasing water turbidity and depth decrease the influence of the bottom reflection on the above-water spectra (Carder et al., 2003; Kutser et al., 2006b; Vahtmäe et al., 2006; Vahtmäe & Kutser, 2013), making the habitat mapping less feasible.

2 Sensors for water remote sensing

A remote sensing sensor has a field-of-view such that at any moment in time, it is viewing a part of Earth's surface and recording how much radiation is being reflected from that part (Philipson, 2003). Remote sensing instrument is most commonly located on either an airborne or space-borne platform. Light giving us information about the properties of sea bottom must pass through the water column and atmosphere before being detected by a sensor (Mumby et al., 2004). The number of classes (categories) distinguishable by remote sensing depends on many factors including, the platform (satellite, airborne, towed instrument), type of sensor (spectral, spatial and temporal resolution), atmospheric clarity, surface roughness, water clarity and water depth (Mumby et al., 2003).

The signal from the water is weak compared to that of the land because water strongly absorbs light nearly at all wavelengths. Sensors built for terrestrial vegetation monitoring are not sensitive enough to measure such small amount of energy and therefore do not give sufficient signal in the case of water bodies. Sensor suitable for water remote sensing require high radiometric resolution and high signal to noise ratio.

A remote sensing sensor can be characterised by its spatial, spectral and radiometric resolution. The spatial resolution of the sensor describes the size of the ground area corresponding to one pixel in the image (Philipson, 2003). A higher spatial resolution will increase the sensors possibility to record spatial detail. Most of the satellites built for water remote sensing (CZCS, SeaWiFS, MODIS, MERIS) are constructed so the revisit time is 2 to 3 days. Therefore, the spatial resolution of these satellites is typically around 1 km. MERIS was more adapted to monitoring coastal waters, and in addition to 1200 m spatial resolution there was high resolution mode with a pixel size of 300 m. Theoretically, the spectral resolution of MERIS would be suitable for mapping benthic habitats (Vahtmäe et al., 2006), but since spatial variability of benthic habitats is usually large, spatial resolution of 300 m is not sufficient.

There are also satellites with very good spatial resolution: IKONOS (4 m), QuickBird (2,4 m), WorldView-2 (2 m). These sensors can be used for mapping benthic habitats (Vahtmäe & Kutser, 2013; Vahtmäe et al., 2011). However, these images are relatively small (about 15x15 km), have to be pre-ordered and the data is more expensive than the data from coarse resolution satellites. Therefore, it is difficult to map very large areas with the high resolution

satellites. Airborne sensors provide high radiometric and spectral resolution and their pixel size depends on flight altitude. Typically, airborne sensors are flown with 1 m or less spatial resolution. Airborne data is usually more expensive per unit of study area than satellite data. On the other hand it contains also much more information.

2.1 RapidEye mission

RapidEye (known as BlackBridge from November 2013) is a commercial Earth Observation system including five satellites, a dedicated SCC (Spacecraft Control Center), a data downlink ground station service, and a full ground segment designed to plan, acquire and process up to 5 million km^2 of imagery every day.

The system is owned and operated by BlackBridge. It is the first fully commercial operational class Earth observation system using a constellation of 5 satellites that provides unparalleled performance. The main parameters of the mission are seen in Table 1. The principal objective is to provide a range of Earth-observation products and services to a global user community. The main vertical markets BlackBridge serves are agriculture, environment, forestry, mapping, intelligence and defense, security and emergency, visual simulation (BlackBridge Homepage; Tyc et al., 2005).

Number of satellites	5
Field of Regard	±20º in cross-track
Ground sampling distance (nadir)	~6.5 m
Swath width	77 km
Global revisit time	1 day
Optical bands	5 (440-850 nm)
Mission design life	> 7 years
Orbit	Sun-synchronous orbit, 630 km

Table 1. Overview of RapidEye mission parameters.

The satellite platforms are being developed and built by Surrey Satellite Technology Ltd., Guildford, Surrey (SSTL). Each RapidEye spacecraft is three-axis stabilized, featuring a box-like shape of approximate dimensions: 0.72 m x 0.75 m x 0.865 m. The overall design has the spacecraft divided into three separate functional volumes. At the base of the spacecraft is the launch vehicle separation system which is lined as a four-point release system with integral

deployment springs along with some attitude sensors. In the mid-deck are the majority of the bus subsystems and the payload electronics unit, while the optical imager and the star camera are located at the top end of the spacecraft (Tyc et al., 2005).

A single launch of the RapidEye minisatellite constellation on a Dnepr launch vehicle took place on August 29, 2008. The launch site was the Baikonur Cosmodrome, Kazakhstan (Surrey Satellite Technology Ltd. Homepage).

The spacecraft follow each other in their orbital plane at about 19 minute intervals (Tyc et al., 2005). A revisit time of one day can be obtained anywhere in the world (±84º latitude) with body pointing techniques. The average coverage repeat period over mid-attitude regions is 5.5 days at nadir (BlackBridge Homepage).

REIS (RapidEye Earth Imaging System) is a multispectral imaging system designed and developed by JOP (Jena-Optronik GmbH). The instrument is also referred to as JSS-56 (Jena-Optronik Spaceborne Scanner-56) as well as MSI (Multispectral Imager) in the literature. REIS is a pushbroom sensor placed on each satellite. Each sensor is capable of collecting image data in five distinct bands of the electromagnetic spectrum (see Table 2). BlackBridge's satellites are the first commercial satellites to include the Red Edge band, which is sensitive to changes in chlorophyll content (BlackBridge Homepage; Tyc et al., 2005).

Channel	**Spectral band name**	**Spectral coverage (nm)**
1	Blue	440-510
2	Green	520-590
3	Red	630-685
4	Red edge	690-730
5	NIR (Near-Infrared)	760-850

Table 2. Spectral bands of RapidEye.

3 Study sites

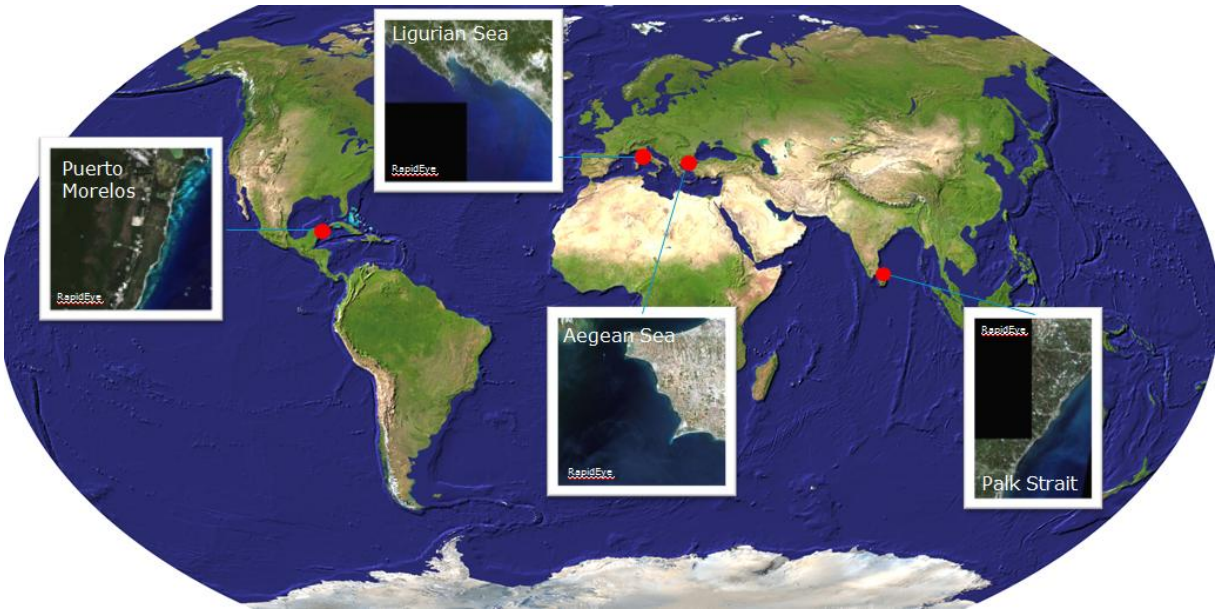

Figure 5. Map of all four study sites.

On Figure 5 is seen the world map, which shows the location of all four selected study sites.

3.1 Puerto Morelos

The Mexian Caribbean is the northern part of the Mesoamerican Reef System, the second largest barrier reef in the world. The nations that border the Caribbean collectively encompass a major global marine biodiversity hot spot (Miloslavich et al., 2010). Puerto Morelos coral reef lagoon (Figure 6) is located on the north-eastern coast of the Yucatan Peninsula, -25 km south of Cancún. Puerto Morelos is a Marine Protected Area (National Marine Park) and Ramsar site no. 1343 (RAMSAR Homepage), covering 91,2 km². The coast of Puerto Morelos is lined by a reef that is about 4 km long, reef lagoon width varies between 550 and 1500 m. The lagoon is relatively shallow, with an average depth of 3-4 m and maximum depth of 8 m (Coronado et al, 2007). The region is routinely under continuous pressure from frequent natural disturbances by hurricanes and tropical storms and due to human impacts of different types and intensities driven mainly by the massive tourism industry (Cerdeira-Estrada et al., 2012). Puerto Morelos region is in the area of influence of the strong Yucatan Current, a microtidal environment and a Trade Wind regime (Sheinbaum et al. 2002; Chavez et al. 2003).

Figure 6. RapidEye image of Puerto Morelos study area.

The bottom of the lagoon is covered by calcareous sand, which is stabilised by seagrass meadows. In certain areas, the underlying calcareous pavement is exposed and colonised by coral reef communities or is covered by unconsolidated carbonate sediments. The reef area is characterised by the presence of shallow wave action. Although the region is microtidal, the reefs may be exposed at low-spring tides (Coronado et al., 2007).

The climate of the region is tropical, with two dominant seasons defined in terms of wind patterns and air temperature. Winter begins in November and continues until March or April. Monthly mean air temperature in winter is 24-25°C, but diurnal minimum can be substantially lower for brief periods following the passages of cold fronts. Monthly resultant wind directions are from the north-eastern quadrant from October to February, although northerly and south-easterly winds occur following the passage of cold fronts. Summer weather patterns are characterised by a dominance of maritime tropical air and frequent thunderstorms. Maximum air temperature is reached in August, with a monthly average of 29°C and maximum above 33°C (Coronado et al., 2007). The average water temperature is 27° C (Ruíz-Rentería et al., 1998).

3.2 Palk Strait

India has a long coastal line of over 7,500 km and an area of 2.02 million km² in exclusive economic zone with very rich biodiversity (Vijayakumar et al., 2007). Palk Strait is an almost enclosed shallow water body that separates Sri Lanka from India (Sivalingam, 2005). The south-western part of the strait is called Palk Bay. The Strait is 64 to 137 km wide, 137 km long and less than 100 m deep. Palk Strait is strategically an important channel, as it is shared by India and Sri Lanka without the scope of international navigation (Gandhi & Rajamanickam, 2004). Since the Strait covers a large area (~17,000 km²), picked study area is in the western part of the water body, part of the coastline of southern India (see Figure 7).

Figure 7. RapidEye image mosaic of Palk Strait study area.

Palk Strait has two openings: on the east into the Bay of Bengal and on the west side into the Gulf of Mannar. The opening on the east is 65 km wide with an average depth of 9.35 m

(lowest point 13 m deep). The opening on the western side is narrower and shallower, interrupted by a larger Pamban Island and other minor sand bars referred to as Adam's Bridge between Pamban Island and western tip of Mannar Island. Compared to the eastern opening, the average depth is less than 1 m, except at the narrow Pamban Pass which is 7 m deep. Both these openings restrict the entry and mixing of fresh oceanic waters. The coastal ecosystem of the strait is endangered by the shallowing nature of the bay due to sedimentation and it is also predicted that the entire bay will be divided into two lagoons by the year of 2040 if the current rate of deposition of sediment is continued (Gandhi & Rajamanickam, 2004).

Palk Strait, being surrounded by dry zone land mass except for the two openings into Bay of Bengal and Gulf of Mannar, has different conditions than the Bay and the Gulf. The few rivers flowing into the Strait causes fluctuation in the salinity of these waters. Salinity values change from 32.8 ppt near the opening to Bay of Bengal to 30.8 ppt near Adam's Bridge and even the value of 29.4 ppt in the southwest corner of the Palk Bay. There is no indication of a definite pattern in the distribution of salinity (Sivalingam, 2005).

Palk Strait is characterized by the absence of hard bottom areas. It is mostly sand and mud, mud and shells or mud only. Most of the shallow areas are full of vegetation. Also long lining trials have indicated that bottom conditions vary considerably within short distances (Sivalingam, 2005).

It is possible to infer that there is no rapid oceanic current movement in either direction within the Palk Strait area. Feature, that confirms absence of current flows is the chlorophyll distribution. Chlorophyll concentration during November and May varies from 3.62 mg/m³ in December to 7.0 mg/m³ in January (Sivalingam, 2005).

3.3 Aegean Sea

The third study area (see Figure 8) is located in north western part of Aegean Sea, Greece. The Aegean Sea is an elongated embayment of the Mediterranean Sea, located between the Greek and Anatolian peninsulas (Wikipedia, Aegean Sea). There is a smooth variance of water depth in the study area and the water is clear. The shallower parts are covered with dense seagrass while the deeper ones are sandy (Doxani et al., 2013).

Figure 8. RapidEye image of Nea Michaniona study area.

Just north of the study area is the second biggest city in Greece –Thessaloniki. The city is built in the heart of Thermaikos Gulf in the Aegean Sea. Thessaloniki is an industrialized modern city of 1.1 million inhabitats, it is the cultural and economic center of Macedonia and northern Greece and an important seaport (Wikipedia, Thessaloniki). Thermaic Gulf is located immediately south of Thessaloniki regional unit. The length of the gulf (north to south) is ~100 km, while its width (east to west) is only ~5 km (Wikipedia, Thermaic Gulf).

The study area lies in a transitional climatic zone, so its climate displays characteristics of several climates. It is a humid subtropical climate, that borders on a semi-arid climate, with annual average precipitation of 450 millimeters. However, the area has a summer precipitation between 20 to 30 millimeters, which borders it close to a hot-summer Mediterranean climate. Winters are relatively dry. During the coldest winters, temperatures can drop to −10 °C, but the coldest month in the area is January and the average temperature then is 6 °C. Wind is also usual in the winter months, with December and January having an average wind speed of 26 km/h. Summers are hot with rather humid nights. Maximum temperatures usually rise above 30 °C, but rarely go over 40 °C. The hottest month of the year in the city is July, with an average temperature of 26 °C (Wikipedia, Thessaoniki).

3.4 Ligurian Sea

The Ligurian Sea is located in the north western part of the Mediterranean Sea. The sea borders with Italy, France and the French island of Corsica. In the east the sea borders the Tyrrhenian Sea and in the west with Mediterranean Sea itself.

The study area (see Figure 9) is in the part of the Ligurian Sea, which borders with southern part of Ligurian region, Italy. Ligurian region is bordered by France on the west, Piedmont on the north and Tuscany on the east. The continental shelf is very narrow and so steep it descends almost immediately to considerable marine depths along its 350-km coastline. There are small beaches, but there are no deep bays and natural harbours except for those of Genoa and La Spezia (Wikipedia, Liguria). La Spezia area and harbour are also part of the study area.

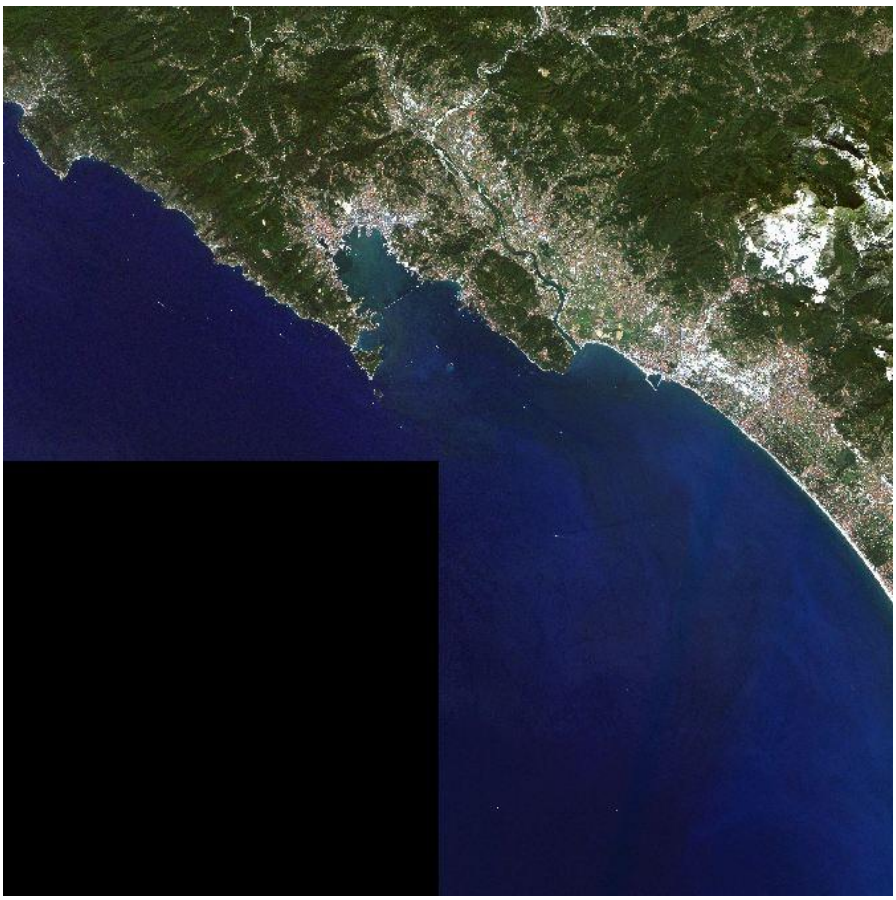

Figure 9. RapidEye image mosaic of Ligurian Sea study area.

Mediterranean seagrass ecosystems are sensitive to local environmental degradation in the form of water clarity, salinity, and temperature variations. These disturbances collectively affect the stability of the ecosystems. In the Mediterranean, seagrass existence is fundamental

in protecting the coastal line from erosion. The regression and/or the disappearance of vegetation in coastal areas heavily modify the sedimentary equilibrium. However, both the anthropogenic impact and changes in natural factors are responsible of the poor condition of seagrass presence (Micheli et al., 2012).

In the study area region, there is also the Cinque Terre area, which includes five coastal villages: Monterosso al Mare, Vernazza, Corniglia, Manarola and Riomaggiore. The coastline, the five villages and the surrounding hillsides are all part of Cinque Terre National Park and is a UNESCO World Heritage Site. The Protected Marine Area was founded in 1997 and preludes the National Park as an effort to protect and maintain proper usage of the sea off the coast of Cinque Terre. It is subdivided into 3 zones, a Strict Nature Reserve, where boaters are prohibited, the General Nature Reserve, which allows access to motor boats, registered retail fishermen and guided scuba diving tours and the last and least stringent Partial Nature Reserve that allows monitored recreational fishing. The coast along the Cinque Terre is characterized by high cliffs, caves, bays, tiny beaches and cleft rocks. Marine life in the stretch of the coast is rich and varied. The *Posidonia oceanica*, a plant that creates very important grass colonies, grows here and provides a safe habitat for the reproduction of many organisms (Wikipedia, Parco Nazionale delle Cinque Terre).

Ligurian sea coastal areas have a typical Mediterranean climate, with hot summers, warm winters and very rainy autumns and springs. The average temperatures of the coldest month January are 4 - 11 °C. In the hottest month July, average temperatures are from 20 °C to 29 °C. Average annual precipitation is 1,314 millimeters. Snow is uncommon, it snows about once or twice a year. In winter the temperatures may fall below zero, reaching about -2 to -10 °C. Conversely, in summer, especially during sunny days, the temperature can easily exceed 30 °C. Furthermore, the sensation of heat in summer is increased by the high humidity (Wikipedia, La Spezia).

4 Materials and Methods

4.1 RapidEye images

RapidEye image products can be bought in different processing levels. Table 3 summarizes the various processing levels of image products (BlackBridge Homepage, RapidEye Products).

Level	Description	Product size
1B	RapidEye Basic Product - Radiometric and sensor corrections applied to the data. On-board spacecraft attitude and ephemeris applied to the data.	Approximately 77 km wide with a variable length of between 50 km and 300 km.
3A	RapidEye Ortho Product - Radiometric, sensor and geometric corrections applied to the data. The product accuracy depends on the quality of the ground control and DEM used.	Tile size is 25km (5000 lines) by 25km (5000 columns).
3B	RapidEye Ortho Take Product – extends the usability of orthorectified RapidEye products by leveraging full image takes and adjusting multiple images together to cover large areas more accurately with fewer files.	Maximum 77 km width by 150 km long.
3M	Mosaic Product. Seamless, color-balanced mosaic made up of orthorectified and bundle-adjusted 1B products.	Standard tile size is 55 km by 55 km.

Table 3. Image processing levels of RapidEye products.

In this study we used Level 3A RapidEye image products. Images were provided by ESA/ESRIN, are chosen and downloaded through BlackBridge EyeFind archive discovery tool. The images are from sensors RapidEye 3 and 5 and all together are downloaded and henceforth processed 13 images from 2011 to 2014 (see Table 4). In the cases of Ligurian Sea and Palk Strait, mosaic images are compiled (accordingly of 3 and 4 same date image products).

The study sites were selected based on ongoing cooperation between ESA and partner insitutions in different countries to get access to *in situ* data from the study areas. The precondition for selecting the images was the fact that they were cloud-free.

Study area	Sensor Type	Date	Image type
Aegean Sea (Greece)	RE3	26.06.2013	Single image
Aegean Sea (Greece)	RE1	12.08.2014	Single image
Ligurian Sea (Italy)	RE4	23.08.2011	Mosaic of 3 images
Ligurian Sea (Italy)	RE5	08.07.2012	Mosaic of 3 images
Palk Strait (India)	RE3	01.01.2012	Mosaic of 4 images
Puerto Morelos (Mexico)	RE3	09.02.2013	Single image

Table 4. The sensor type and date of used image products and mosaics.

4.2 Image processing

Image processing started with making the mosaics, if needed, and building and applying land masks to all images. For these operations software ENVI 4.8 was used. Mosaics were built to enlarge the study area and land masks are built and applied to loose the unnecessary part of the image – land. Processing chain is shown on Figure 10.

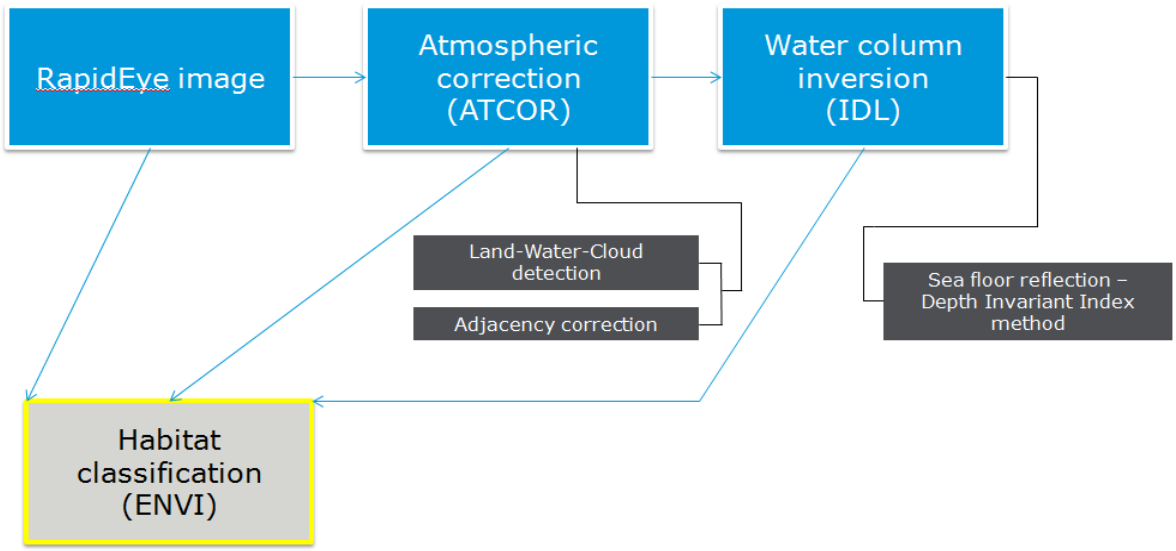

Figure 10. Image processing chain in this study.

4.2.1 Atmospheric correction in ATCOR

Imagery collected by the satellites are largely contaminated by the effects of atmospheric particles through absorption and scattering of the radiation from the earth surface. The objective of atmospheric correction is to retrieve the surface reflectance (that characterizes the surface properties) from remotely sensed imagery by removing the atmospheric effects. Atmospheric correction has been shown to significantly improve the accuracy of image classification (UMIACS, Atmospheric correction, 1995).

Atmospheric correction was performed using ATCOR-2/3, which is based on MODTRAN-4. MODTRAN (MODerate resolution atmospheric TRANsmission) is a computer program designed to model atmospheric propagation of electromagnetic radiation (Wikipedia, MODTRAN). ATCOR-2 is generally used to atmospherically correct data from optical spaceborne sensors assuming flat terrain conditions. ATCOR-3 accounts for terrain effects by incorporating DEM data and their derivatives such as slope and aspect, sky view factor and cast shadow. ATCOR-3 is therefore suitable for atmospheric correction of sensor data acquired over rugged terrain (ATCOR Homepage). Therefore in this study ATCOR-2 module for flat terrains in software ATCOR-2/3 is used.

Land was masked out on all RapidEye imagse used in this study. Parameters that needed to be specified manually were: image acquisition date, sensor type (its calibration file is automatically found after selecting correct type), satellite azimuth angle and solar azimuth angle (found in the metadata file), tilt angle (calculated from satellite and solar azimuth angles) and atmospheric file (for example for study area in Puerto Morelos, it is tropical maritime). Pixel size and visibility are firstly selected automatically after putting in other parameters, but can be changed manually before starting the atmospheric correction process. Visibility can also be automatically changed throughout the process, but before changing it the program asks permission for that.

If all the parameters are specified or automatically chosen, atmospheric correction can be done. On the Figure 11 an example of original image and the same image after land masking and atmospheric correction are shown.

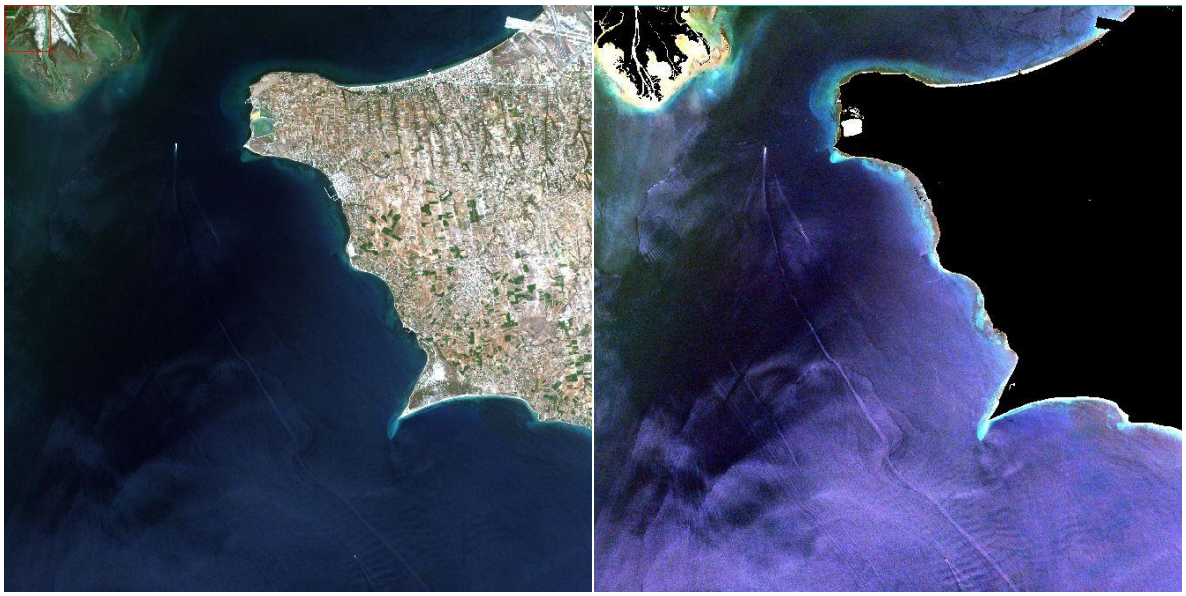

Figure 11. Original RapidEye true colour image product on the left and land masked atmospherically corrected image product on the right. Aegean Sea study area (2014).

4.2.2 Depth Invariant Index method in IDL

Depth-Invariant Index method is image-based approach to compensate for the effect of variable depth when mapping bottom features. Rather than predicting the reflectance of the seabed, which is prohibitively difficult, the method produces a "depth-invariant bottom index" from each pair of spectral bands.

The method has two main requirements, which are that it needs optimal two bands (green (i) and blue (j) band) and attenuation coefficients of specific wavelengths are needed (UNESCO, Water Column Correction Techniques).

Depth-Invariant Index expressed as a formula:

$$depth - invariant\ index_{ij} = \ln(L_i) - \left[\left(\frac{k_i}{k_j}\right)\ln(L_j)\right],$$

where L_i is the pixel radiance in band *i* (green), k_i/k_j is the ratio of attenuation coefficients and L_j is the pixel radiance in band *j* (blue) (UNESCO, Water Column Correction Techniques).

Code for applying this formula to each image (or some cases mosaic) separately is written in IDL. The input image for this method is atmospherically corrected land masked RGB image.

On the Figure 12 are seen the processes of Depth-Invariant Index method.

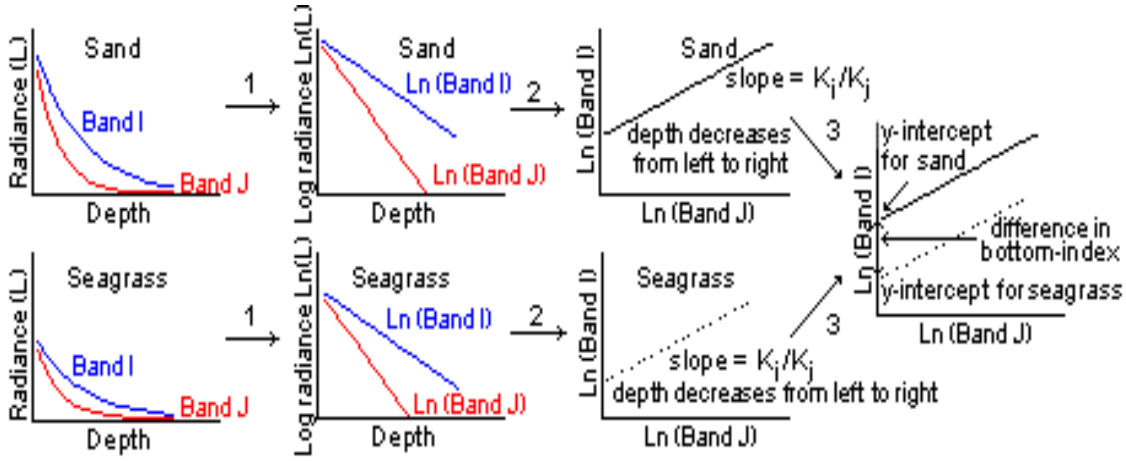

Figure 12. Processes of Depth-Invariant Index method, showing the steps involved in creating depth-variant indices of bottom type for sand and seagrass.

Firstly the exponential attenuation of radiance with depth linearised for band *i* and *j* using natural logarithms. As seen on the Figure 12 band *i* has a shorter wavelength, and therefore attenuates less rapidly, than band *j*. Moving to the second step, a plot of (transformed) band *i* against (transformed) band *j* for a unique substratum at various depths is seen. Gradient of line represents the ratio of attenuation coefficients, k_i / k_j. The ratio is the same irrespective of bottom type. If reflectance values from different bottom type were added to the bi-plot, as seen in the step 3, a similar line would be obtained. The only change between data points would be because of the depth difference. An index of bottom type can be obtained by noting the *y*-intercept for each bottom type (UNESCO, Water Column Correction Techniques). On the Figure 13 is seen an example of atmospherically corrected image before Depth-Invariant Index method applied and after the method applied.

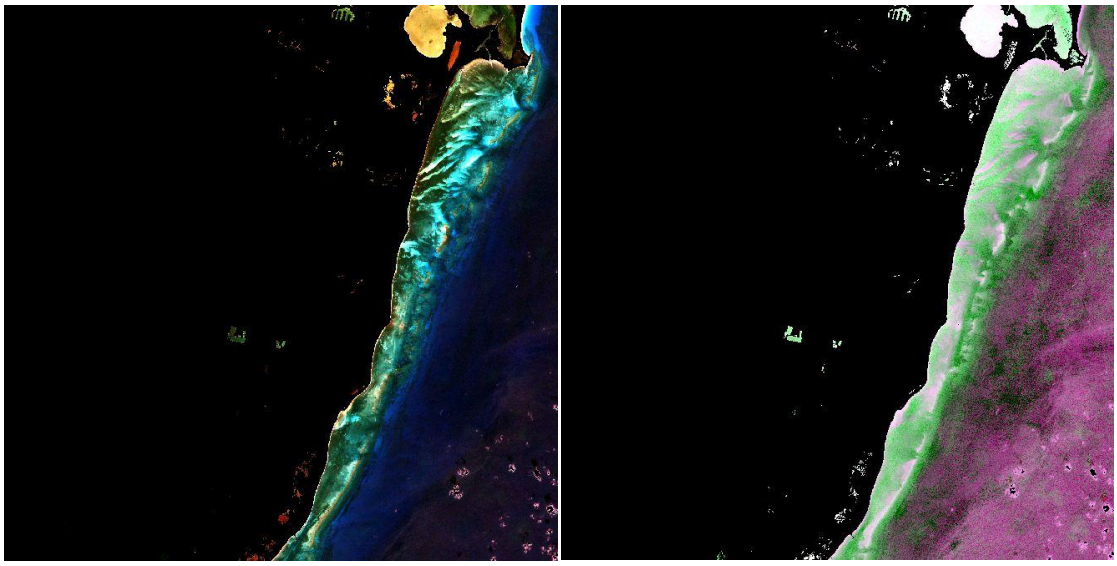

Figure 13. Atmospherically corrected image product on the left and Depth-Invariant Index method applyed image product on the right. Puerto Morelos study area.

4.2.3 Classification of bottom types in ENVI

There are several approaches in classifying remote sensing imagery collected above the shallow water. For example, unsupervised classification methods can be used to divide the study area into as many classes as statistically feasible and then name the classes afterwards using either *in situ* data or other knowledge about the study site. If *in situ* data is available then one may use supervised classification using the information from the sampling points as class parameters. The disadvantage of both of those methods is need in large amount of *in situ* data and non-transferability of the results from study site to study site and from one satellite to another. An alternative approach (called physics based or analytical method) is using measured or modelled spectral library and supervised classification methods (Kutser & Jupp, 2002; Kutser et al., 2006a). The advantage of this method is that no *in situ* data collected simultaneously with satellite overpass is needed, both water depth and bottom type information can be retrieved simultaneously, and the method is easily transferable to different types of sensors. The disadvantage is high requirement to accuracy of atmospheric correction of the imagery.

After land masking, atmospheric correction of the images, and using the Depth-Invariant Index method on them, classification in ENVI 4.8 was carried out. The original RapidEye imagery, atmospherically corrected imagery and Depth-Invariant Index imagery was used in the study.

The study sites were selected based on ongoing cooperation between ESA and partner institutions in different countries. We planned to use these connections to get access to *in situ* data from the study sites. Unfortunately, we weren't able to receive *in situ* data from any of the study sites up to know and therefore it was not possible to use classification methods that need *in situ* data. The *in situ* data is also needed for evaluating classification errors. This was not possible either.

In each image the pixels were visually classified into as many different categories as possible based on pixel spectra. Each Region of Interest (ROI) selected consisted of at least 9-12 pixels. After selecting pixels into ROIs, different supervised classification options were used. ENVI has several options for supervised classification: Minimum Distance, Maximum Likelihood, Mahalanobis Likelihood and Spectral Angle Mapper (ENVI User Guide, Supervised Classification). In this study Minimum Distance and Spectral Angle Mapper classification modules were used.

The Minimum Distance (MD) technique uses the mean vectors of each endmember and calculates the Euclidean distance from each unknown pixel to the mean vector for each class. All pixels are classified to the nearest class unless a standard deviation or distance threshold is specified, in which case some pixels may be unclassified if they do not meet the selected criteria (ENVI User Guide, Minimum Distance Classification).

Spectral Angle Mapper (SAM) is a physically-based spectral classification that uses an *n*-D angle to match pixels to reference spectra. The algorithm determines the spectral similarity between two spectra by calculating the angle between the spectra and treating them as vectors in a space with dimensionality equal to the number of bands. This technique, when used on calibrated reflectance data, is relatively insensitive to illumination and albedo effects. SAM compares the angle between the endmember spectrum vector and each pixel vector in *n*-D space. Smaller angles represent closer matches to the reference spectrum. Pixels further away than the specified maximum angle threshold in radians are not classified (ENVI User Guide, Spectral Angle Mapper Classification).

4.2.4 Using Spectral Library for classification

In the spectral library approach, remote sensing reflectances of individual image pixels are compared to simulated remote sensing spectra created using measured values of bottom reflectance and water inherent optical properties (Vahtmäe & Kutser, 2013). As said previously, the advantage of using this approach is that it does not require extensive field surveys, but on the other hand, the optical properties of benthic substrates and optical properties of the water column have to be known. Also, using this method, requires high quality of atmospheric correction (Kutser et al., 2006a).

The spectral library used in this study was compiled based on Estonian optical properties of relatively clear water. The radiative transfer numerical model, HydroLight 5.0, was used to predict the reflectance of different bottom types above the water surface depending on their depth and optical water properties. This model uses optical properties of the water column, sea surface state, bottom albedo and sky conditions to obtain the radiance distribution within and leaving a water body. Input data for HydroLight was collected during the field campaign near Vilsandi Island and included water constituents, such as chlorophyll, coloured dissolved organic matter and suspended matter, benthic reflectance without overlaying the water column and local environmental conditions, such as the day, time, wind speed and cloud cover (Vahtmäe & Kutser, 2013).

The spectral library modeled by HydroLight was calculated for the bottom reflectance spectra of sand, brown algae (Fucus vesiculosus), red algae (Ceramium tenuicorne), green algae (Cladophora glomerata). Each bottom reflectance was modelled at depths from 1 m to 6 m in 1 m intervals and also at depths 0.1 m and 0.5 m with spectral interval of 5 nm from 350 nm to 850 nm. The output provides an estimate of the remotely sensed signal, including both the effects of bottom brightness and water column contribution. An optically deep water spectrum was also included, describing the reflectance expected from the water column alone with no influence from the benthos.

RapidEye minisatellites have five spectral bands (seen in Table 2). The hyperspectral library was recalculated for RapidEye bands by calculating average value of each band width. The spectra that formed the RapidEye spectral library and were used in image processing are seen below (Figures 14-18).

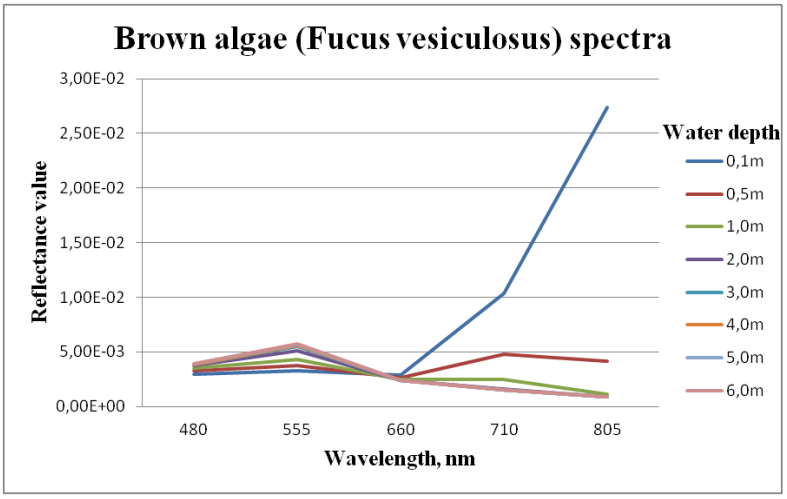

Figure 14. Brown algae (Fucus vesiculosus) spectra calculated for different water depths RapidEye bands.

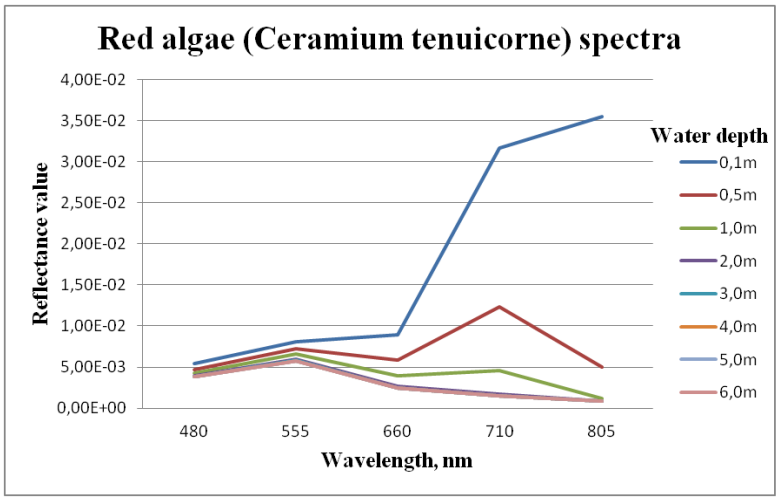

Figure 15. Red algae (Ceramium tenuicorne) spectra calculated for different water depths and RapidEye bands.

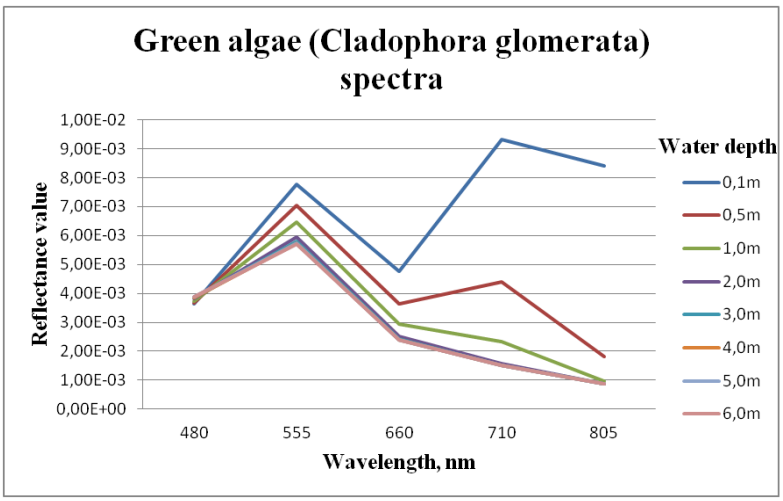

Figure 16. Green algae (Cladophora glomerata) spectra calculated for different water depths and RapidEye bands.

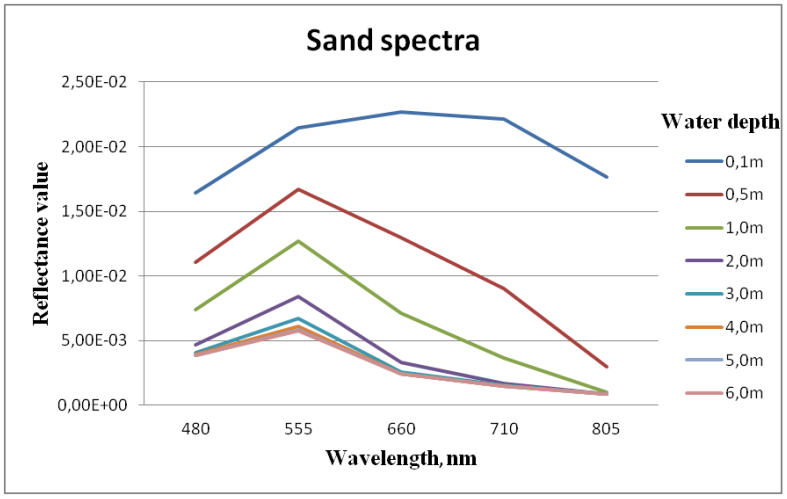

Figure 17. Sand spectra calculated for different water depths and RapidEye bands.

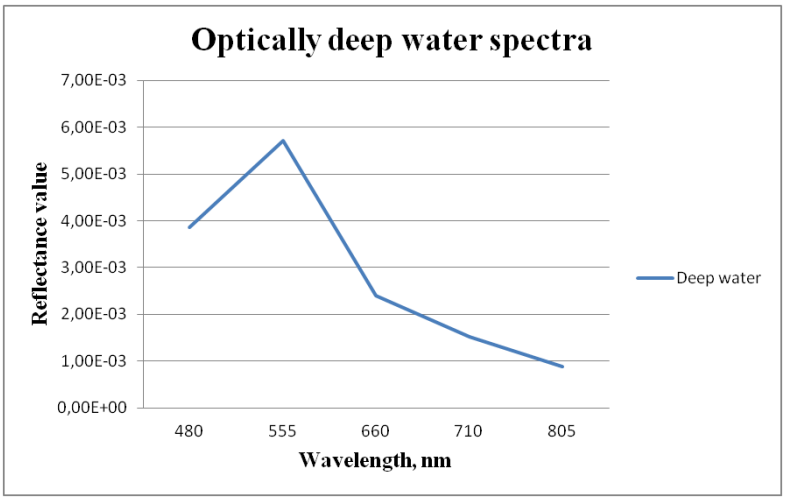

Figure 18. Deep water spectra calculated for RapidEye bands.

5 Results and discussion

As said in the previous chapter, the last step of the processing chain, classification of the bottom types, was done for land masked original RapidEye images, images which have gone through atmospheric correction and images which have also gone through Depth-Invariant Index method processing.

At first, we used the spectral library created for the RapidEye (Chapter 4.2.4) and Spectral Angle Mapper to produce benthic habitat maps. This would have helped to overcome the problem of absence of *in situ* data from the study sites. Unfortunately, these efforts did not produce credible results. One of the problems may be optical water properties used in the model. We used optical properties from our clearest water site near Vilsandi Island, but the study sites were in clearer waters. Other problem may be spectral similarity of the bottom types. It was described above that the spectral features characteristic to different groups of benthic algae are narrow and not detectable by multispectral satellites with a few wide spectral bands. This may have been other reason for the poor results.

As a next step two supervised classification methods – Minimum Distance method and Spectral Angle Mapper were used to produce benthic habitat maps when the spectral library method failed. The methods were applied on the original, atmospherically corrected and depth invariant images. Consequently, we have six benthic habitat maps as outcome for all four study sites.

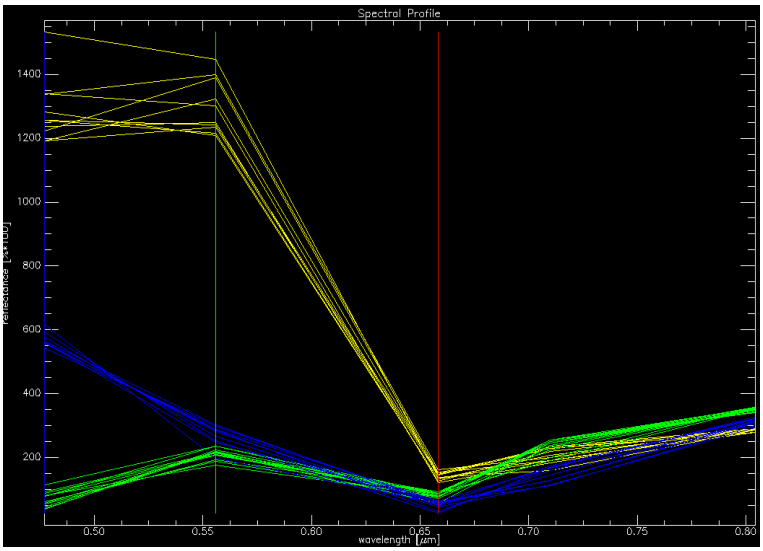

Figure 19. Spectra of three different classes of pixels collected from the atmospherically corrected image of the Puerto Morelos study area.

Three types of spectra were identifiable on the Puerto Morelos image: one is brighter than the others, second one is decreasing with increasing wavelength in the visible part of spectrum and the third has maximum values in the green part and relatively high values in the near-infrared part of the spectrum. Spectra of the three classes are shown in Figure 19.

Comparing the spectra found in the area with spectra published in the literature and with the modelled spectral library shown in Figures 14-17, one can conclude that the yellow class is bright sea bottom with no or little vegetation. It is known that in the Puerto Morelos area there are two main types of sea bottom: sand and seagrass. Therefore, it is likely that the first class in the classification products, marked with yellow, is bright calcareous sand with no or little vegetation. Chlorophyll containing plants and animals (such as corals) absorb light in the blue part of the spectrum and have higher reflectance values in the green and near-infrared part of spectrum. The green spectra shown in Figure 19 are typical vegetation spectra. It is known from Coronado et al. (2007), that seagrass is the dominating vegetation type of this area. Therefore, it can be concluded that the vegetation class (green) represents seagrass communities. The blue spectra in Figure 19 resemble optically deep water spectra that have higher values in blue part of spectrum and decreasing reflectance with increasing wavelength. Optically deep water reflectance should approach zero in infrared part of spectrum due to strong absorption of light by water molecules. The non-negligible reflectance of the deep water spectra indicates that the RapidEye images contain sun glint.

Figures 20 and 21 are showing the classification results of the Puerto Morelos area.

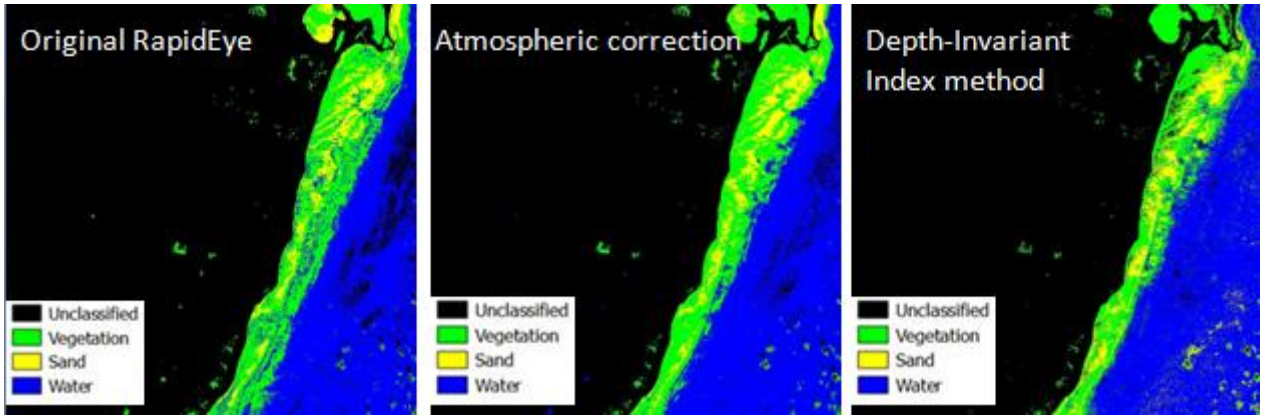

Figure 20. Bottom types of Minimum Distance classification products of the Puerto Morelos study area.

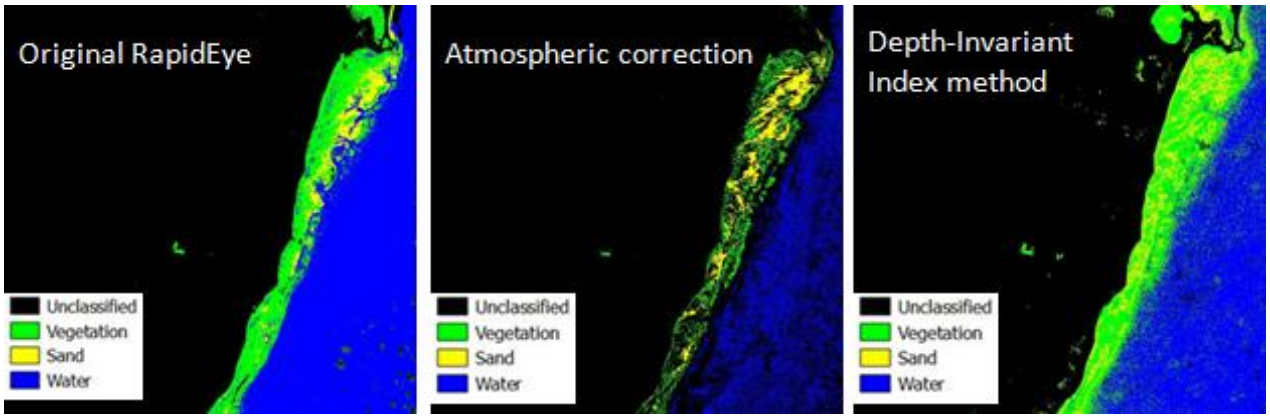

Figure 21. Bottom types of Spectral Angle Mapper classification products of the Puerto Morelos study area.

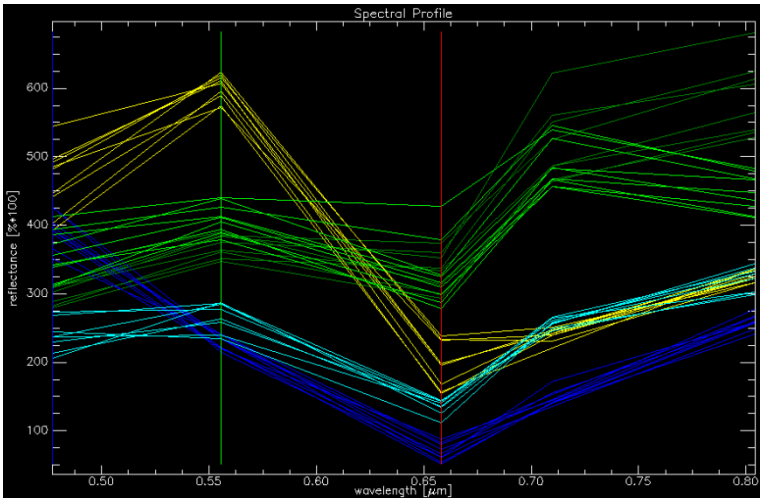

Figure 22. Spectra of five different classes of pixels collected from atmospherically corrected image of the Palk Strait study area.

It was possible to identify five spectrally distinct classes on the Palk Strait image. Deep water and sand spectra were similar to the classes identified in the Puerto Morelos image. However, there were three different vegetation classes identifiable in the image. The main difference between the two vegetation classes was in brightness (reflectance values). Most of the spectral features, that allow differentiation between red, green, brown algae and higher order vegetation, are in the red part of spectrum (Kutser et al., 2003; Kutser et al., 2006b). These spectral differences cannot be resolved with RapidEye spectral resolution. Therefore, it is nearly impossible to determine in the absence of *in situ* data which vegetation types we were able to classify in the Palk Strait image. The two subclasses of the green class (light green and dark green in Figure 22) may be the same type of vegetation at different depths as absorption by water molecules increases exponentially with increasing wavelength in near-infrared part of spectrum and the decrease in light green spectra at 805 nm may be caused by slightly deeper water.

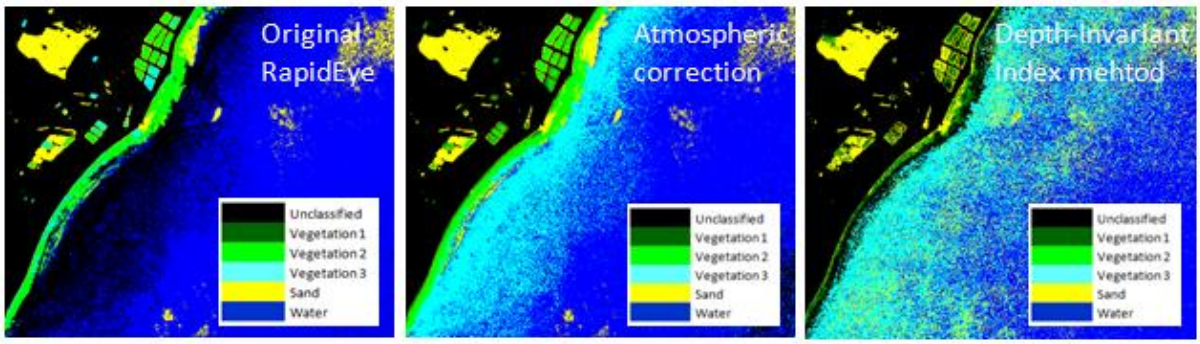

Figure 23. Bottom types of Minimum Distance classification products of the Palk Strait study area.

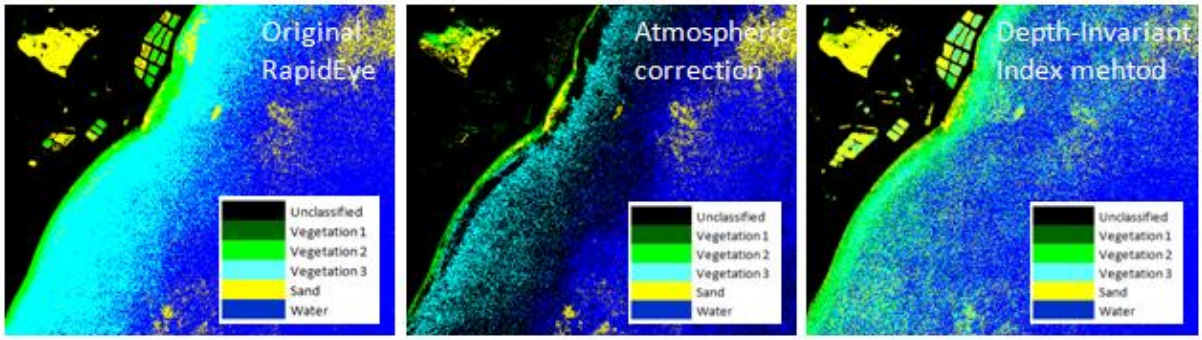

Figure 24. Bottom types of Spectral Angle Mapper classification products of the Palk Strait study area.

The Palk Strait study area classification products are shown in Figures 23 and 24. There are lot of vegetation pixels in supposedly deep water areas in the Depth-Invariant Index method classification results produced by both MD and SAM classification method.

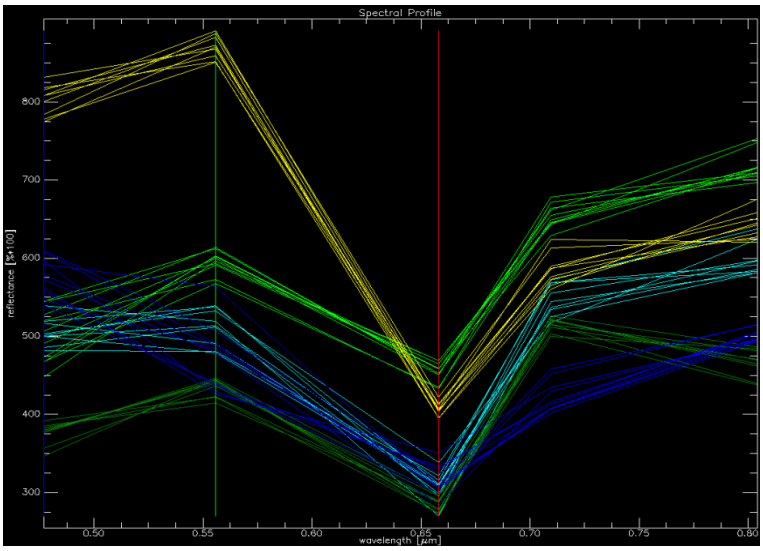

Figure 25. Spectra of five different classes of pixels collected from atmospherically corrected image of the Aegean Sea study area.

The spectra of the Aegean Sea study area pixels are shown in Figure 25. The sand and deep water spectra found in the Aegean Sea image are similar to those of previous study sites. Only

the contribution of glint is slightly higher as the near-infrared signal in sand and deep water spectra is higher than in the previous study sites. The glint is also clearly visible in the atmospherically corrected image (Figure 11). The number of vegetation classes found in the Aegean Sea image was three. As was mentioned above, it is practically impossible to make any decisions about what kind of vegetation types were spectrally resolvable without having any *in situ* data and having too few spectral bands. Comparison with the modelled spectral library spectra (Figures 14-18) did not allow determining the three vegetation classes either. It is known from Doxani et al. (2013) that seagrass is the dominating vegetation type of this area. Therefore, it can be concluded that one of the three vegetation class represents seagrass communities.

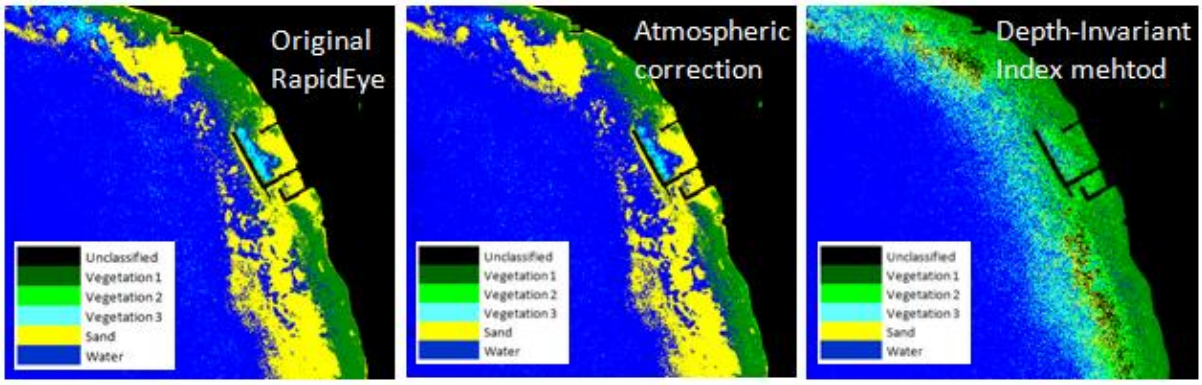

Figure 26. Bottom types of Minimum Distance classification products of the Aegean Sea study area (2014).

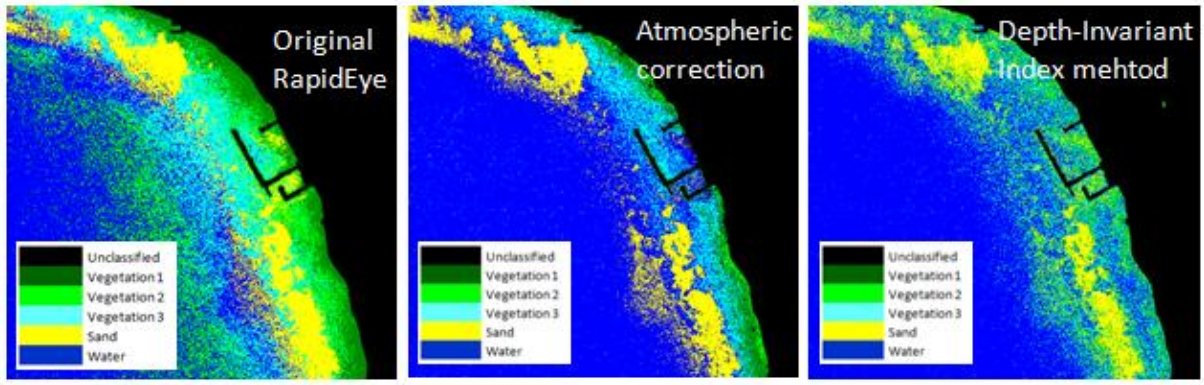

Figure 27. Bottom types of Spectral Angle Mapper classification products of the Aegean Sea study area (2014).

It seems that the MD classification method image is again showing vegetation pixels, where it should be optically deep water in case of the Depth-Invariant Index method image.

Comparing the classification results between MD and SAM methods (Figures 26 and 27), one can say that the MD classification method produces more reliable results, since the

classification maps produces with SAM show large number of vegetation pixels in the areas where water should be too deep to see any vegetation.

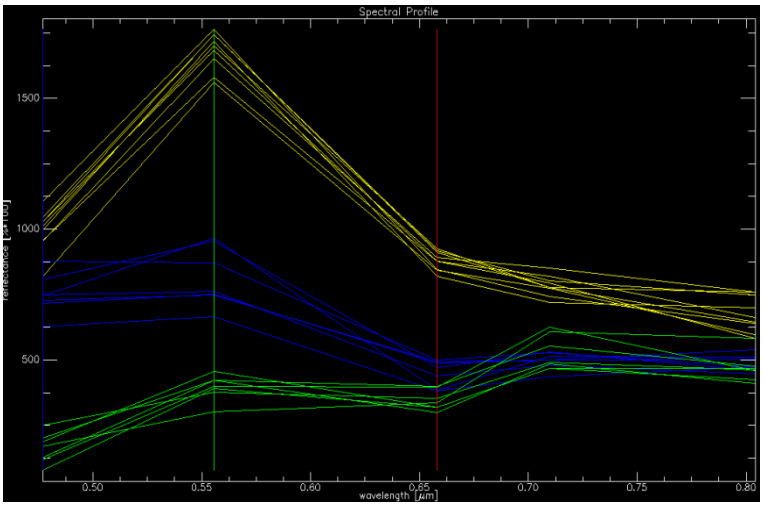

Figure 28. Spectra of three different classes of pixels collected from atmospherically corrected image of the Ligurian Sea study area.

The Ligurian Sea image can be classified into three classes: sand, optically deep water and vegetation, based on the reflectance spectra (shown in Figure 28). The sand and deep water spectra contain relatively little glint compared to the previous study sites. Also the deep water spectra indicate slightly more turbid water as the values in the blue band are relatively not so high (compared to green band) as in the previous study sites. The information available in literature suggest that the vegetated areas are probably covered by seagrass (Micheli et al., 2012).

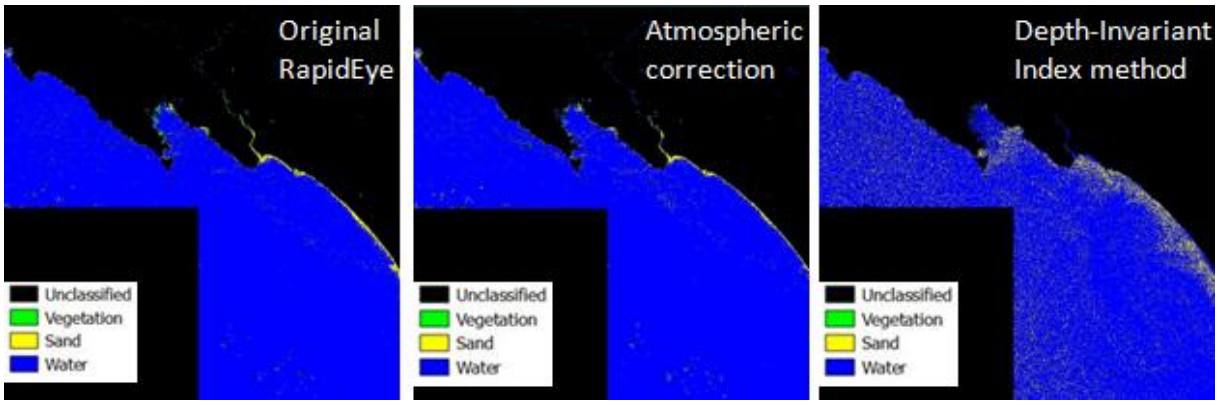

Figure 29. Bottom types of Minimum Distance classification products of the Ligurian study area (2012).

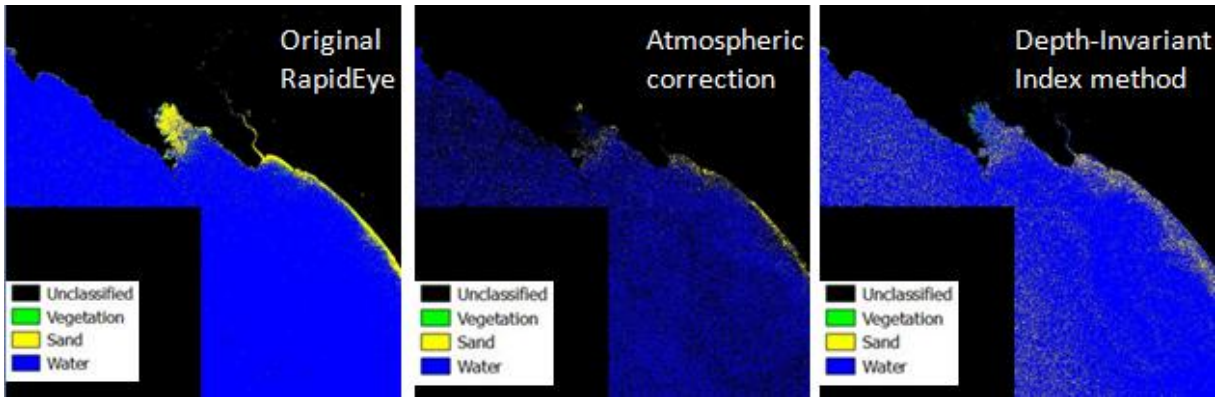

Figure 30. Bottom types of Spectral Angle Mapper classification products of the Ligurian Sea study area (2012).

Figures 29 and 30 show the classification products of Ligurian Sea area. This area has very narrow shallow area near the coast-line and the water depth increases rapidly. In both MD and SAM classification method cases the Depth-Invariant Index method images are again showing a lot of vegetation pixels in the area where water is probably optically deep.

Comparing the classification results between MD and SAM methods, it can be inferred that better results for this study sites are acquired, using MD classification method as in case of all the previous study sites.

Sand pixels brightness is relatively higher than that of any bottom type with vegetation cover. Therefore, it was relatively straightforward to identify sand pixels in RapidEye imagery from all study sites. Vegetation pixels have a peak in the green band and high values in the near-infrared part of spectrum. Comparisons with spectra found in relevant publications and with the modelled spectral library presented in Figures 14, 15 and 16 allow to determine which pixels represent vegetation. However, absence of the *in situ* results and poor spectral resolution of RapidEye do not allow to classify the bottom types more precisely even if we know that up to three vegetation classes were separable in some of the studied imagery. Deep water spectra from clear study sites were relatively easily separable from vegetation due to the maximum in blue part of spectrum. However, this will not be the case in more turbid or CDOM-rich water as both phytoplankton and CDOM absorb light strongly in the blue band and in such waters the deep water reflectance may resemble vegetation spectra. It is seen in the modelled spectral library spectra (Figures 14-18) that in the Baltic Sea all vegetation types look spectrally almost inseparable when water is just 4-5 m deep. Water transparency was probably higher in all the RapidEye study sites. However, modelling results for clear oceanic waters (Kutser et al., 2006a) show that in the red part of spectrum (where most of the useful

signal is) different bottom types become nearly identical to deep water spectra in just 5-6 m deep waters.

In two of the four study areas, Aegean Sea and Palk Strait, the vegetated areas were classified into three different classes based on their optical spectra. In other two areas, spectra showed only one type of vegetation. The number of classes detectable in different sites is most probably related to the actual number of vegetation types available. For example, coastal regions with sand and seagrass meadows with one dominating class of seagrass are quite common. In that case it cannot be expected that RapidEye (or any other remote sensing instrument) can separate more than one vegetation class. In such areas it is possible to map seagrass density from remote sensing imagery (Dierssen & Zimmerman, 2003), but the differences in density are then seen as variation in brightness (reflectance values) not in the spectral shape.

Spectral resolution RapidEye minisatellites is similar to that of Landsat satellites. Landsat series satellites have been used in benthic habitat mapping with relatively good results (Lyons et al., 2012; Palandro et al., 2008). RapidEye has better spatial resolution than Landsat (6,5 m compared to 30 m). Therefore, RapidEye should provide better results in the areas where there is relatively variable sea bottom. Unfortunately, it was not possible to compare the accuracy of RapidEye with Landsat or other multispectral satellites (SPOT, QuickBird, WorldView-2, IKONOS) due to the absence of *in situ* data from the study sites.

Summary

Benthic habitats are important components of coastal zone ecosystem. The vegetation contributes to the primary production in coastal areas, supporting grazing and detrital food webs. Aquatic vegetation is also providing food, spawning and nursery grounds for fishes and other invertebrate species. Benthic vegetation helps to prevent coastal erosion by binding sediments and reduces nutrient loading and other forms of pollution.

The objective of this Master thesis was to study whether RapidEye satellite imagery is suitable for mapping benthic algal cover in shallow water coastal environment.

There were four study sites in different places of the world (Mexico, India, Creece and Italy).

Different classification methods were tested – unsupervised classification, modelled spectral library and supervised classification method with visually selected classes. Unsupervised classification requires *in situ* data to name each class on the image product. Unfortunately, we were not able to acquire any *in situ* data from the study sites before submission deadline of this thesis. Analytical methods, based on modelled spectral library, do not require *in situ* data collected (nearly) simultaneously with satellite overpass. We tested a modelled spectral library in interpreting RapidEye data. The results were not promising. The main reason is probably the difference between the optical properties of water column in a clear Baltic Sea site (used in the model) and the actual water properties in the study sites, as the optical properties of different benthic algal groups are relatively consistent globally. Finally, supervised classification and visually selected classes were used to test RapidEye performance. The visual selection was based on reflectance spectra collected from atmospherically corrected images. Sand and deep water spectra were easily identifiable comparing the spectra with modelled spectral library and spectra available in literature. It was not possible to identify vegetation classes (1-3 depending on study site) not having the *in situ* data.

Three different types of imagery (original radiance, atmospherically corrected and Depth-Invariant) and two classification methods (Minimum Distance and Spectral Angle Mapper) were used. It was not possible to calculate classification accuracies for each class not having the *in situ* data. However, the results indicate that using the original image and Minimum Distance methods seemed to produce the most realistic results.

Madala rannikuvee põhjataimestiku kaardistamine RapidEye satelliidipiltide põhjal

Laura Lõugas

Kokkuvõte

Põhjataimestik on oluline komponent rannikualade ökosüsteemis. Veealune taimestik on toiduks, kudemis- ja kasvualaks kaladele ja teistele selgrootutele. Põhjataimestik aitab takistada rannikuerosiooni, vähendab toitainete üleküllastumist rannikuvees ja muud liiki reostusi.

Käesoleva töö eesmärgiks oli uurida, kas RapidEye satelliidiprodukte saab kasutada põhjataimestiku kaardistamiseks madalates rannikuvetes. Välja oli valitud neli uuritavat ala erinevates maailma paikadest (Mehhiko, India, Kreeka ja Itaalia).

Piltide töötlemisel rakendati juhendamata klassifikatsiooni, modelleeritud spektrikogudel põhinevat analüütilist meetodit ning juhendatud klassifikatsiooni meetodit, kus klassid olid defineeritud iga uurimispiirkonna pildil spektreid analüüsides. Esimesed kaks meetodit ei andnud positiivseid tulemusi. Juhendamata klassifikatsiooni puhul on vaja *in situ* andmeid iga klassi defineerimiseks. Kahjuks ei õnnestunud ühestki uurismipiirkonnast magistritöö esitamise ajaks kontaktandmeid saada. Analüütilise meetodi puhul kasutasime Läänemere optiliste omaduste baasil loodud spektrikogu. Tõenäoliselt ei sobinud see uuritavate piirkondade jaoks kus vesi on palju selgem. Seejärel rakendati pilditele kahte erinevat juhendatud klassifikatsiooni meetodit – minimaalne vahemaa (Minimum Distance) ja spekraalse nurga kaardistaja (Spectral Angle Mapper) kasutades iga konkreetse uurimispiirkonna atmosfäärikorrektsiooniga pildil defineeritud klasse. Liiva ja sügava vee klassid olid selgesti identifitseeritavad võrreldes pildilt saadud vee heleduskoefitsiendi spektreid modelleeritud spektrikogu ja kirjandusest leitud spektritega. Taimestiku klass oli samuti selgesti sügavast veest ja liivast eristatav. Erinevates uurimispiirkondades oli 1-3 erinevat taimestiku klassi üksteisest eristavad. RapidEye spektraalse lahutuse juures ning omamata kontaktandmeid oli võimatu öelda millise konkreetse põhjataimestiku tüübi võiks siduda RapidEye pildilt leitud taimestiku klassiga. Erandiks olid siin uurimispiirkonnad kus on teada, et kasvab põhiliselt merihein ning kui RapidEye pildilt ei tuvastatud rohkem taimestiku klasse kui üks. Kuue erineva tulemuse võrdlemise põhjal võib öelda, et minimaalse vahemaa klassifikatsiooni meetod koos RapidEye toorpiltidega annab antud nelja uuritava ala põhjal usaldusväärsemaid tulemusi.

Acknowledgements

The author is very grateful to the supervisor Tiit Kutser for his professional supervision throughout the work of this thesis. Rapid feedback, help and recommendations made possible the smooth completion of the Master thesis.

Author also likes to thank Gordon Campbell, who was her supervisor during the traineeship in ESA/ESRIN in Italy from February 2014 to January 2015. During this traineeship RapidEye data was selected and downloaded and these images are provided by ESA/ESRIN. ESA/ESRIN also provided the licence of using ATCOR software for atmospheric correction.

References

Anstee, J., Dekker, A., Byrne, G., Daniel, P., Held, A., Miller, J. (2000). Use of hyperspectral imaging for benthic species mapping in South Australian coastal waters. 10th Australasian Remote Sensing and Photogrammetry Conference, Adelaide, 1051-1061.

ATCOR Homepage, http://atcor.com/products/atcor/index.html, 18.03.2015.

Barale, V., Folving, S. (1996). Remote sensing of coastal interactions in the Mediterranean region. *Ocean & Coastal Management*, 30, 217-233.

BlackBridge Homepage, http://www.blackbridge.com/rapideye/index.html, 03.11.2014.

BlackBridge Homepage, RapidEye Products, http://www.blackbridge.com/rapideye/products/index.html, 21.02.2015.

Bukata, P. R., (2005). Satellite monitoring of inland and coastal water quality: retrospection, introspection, future direction. Taylor and Francis Group, Boca Raton, 5-60 pp.

Bukata, R. P., Jerome, J. H., Kondratyev, K. Y., Pozdnyakov. (1995). Optical Properties and Remote Sensing of Inland and Coastal Waters. CRC Press, Ontario.

Carder, K. L., Liu, C., Lee, Z., English, D. C., Patten, J., Chen, F. R., Ivey, J. E. (2003) Illumination and turbidity effects on observing faceted bottom elements with uniform Lambertian albedos. *Limnology and Oceanography*, 48, 355-363.

Cerdeira-Estrada, S., Heege, T., Kolb, M., Ohlendorf, S., Uribe, A., Muller, A., Garza, R., Ressl, R., Aguirre, R., Marino, I., Silva, R., Martell, R. (2012). Benthic habitat and bathymetry mapping of shallow waters in Puerto Morelos reefs using remote sensing with a physics based data processing. Geoscience and Remote Sensing Symposium (IGARSS), 2012 IEEE International, 22-27 July 2012.

Chávez, G., Candela, J., Ochoa, J. (2003). Subinertial flows and transports in Cozumel Channel. *Journal of Geophysixal Research: Oceans*, 108, C2.

Coronado, C., Candela, J., Iglesias-Prieto, R., Sheinbaum, J., López, M., Ocampo-Torres, F. J. (2007). On the circulation in the Puerto Morelos fringing reef lagoon. *Coral Reefs*, 26, 149-163.

Dekker, A. G., Malthus, T. J. Goddijn, L. M. (1992). Monitoring cyanobacteria in eutrophic waters using airborne imaging spectroscopy and multispectral remote sensing system. Proc. 6th Australasian Remote Sensing Conf., Wellington, 1, 204-214.

Dekker, A.G., Brando, V.E., Anstee, J.M., Pinnel, N., Kutser, T., Hoogenboom, E.J., Peters, S., Pasterkamp, R., Vos, R., Olbert, C., Malthus, T.J.M. (2001). Imaging spectrometry of water. In: *Imaging Spectrometry: Basic principles and Prospective Applications* (Eds. F. D van der Meer, S. M. De Jong), Kluwer Academic Publishers, Drodrecht.

Dennison, W.C. (1987). Effect of light on seagrass photosynthesis, growth and depth distribution. *Aquatic Botany*, 27, 15–26.

Dennison, W.C., Orth, K.A., Moore, R.J., Stevenson, J.C., Carter, V., Kollar, S., Bergstrom, P.W., Batiuk, R.A. (1993). Assessing water quality with submersed aquatic vegetation. *Bioscience*, 43, 86–94.

Dierssen, H. M., Zimmerman, R. C. (2003). Ocean color remote sensing of seagrass and bathymetry in the Bahamas Banks by high-resolution airborne imagery. *Limnology and Oceanography*, 48, 444-455.

Doxani, G., Papadopoulou, M., Lafazani, P., Tsakiri-Strati, M., Mavridou, E. (2013). Sun glint correction of very high spatial resolution images. Thales, in honor of Prof. Emeritus Michael E. Contadakis, ISBN 978-960-89704-1-0, p. 329-340.

ENVI User Guide, Minimum Distance Classification,

http://www.exelisvis.com/docs/minimumdistance.html, 20.03.2015.

ENVI User Guide, Spectral Angle Mapper Classification,

http://www.exelisvis.com/docs/spectralanglemapper.html, 20.03.2015.

ENVI User Guide, Supervised Classification,

http://www.exelisvis.com/docs/Classification.html#ClassSupervised, 20.03.2015.

Fonseca, M. (1989). Sediment stabilization by Halophila decipiens in comparison to other seagrasses. *Estuarine, Coastal and Shelf Science*, 29 (5), 501-517.

Fornes, A., Basterretxea, G., Orfila, A., Jordi, A., Alvarez, A., Tintore, J. (2006). Mapping Posidonia oceanica from IKONOS. *ISPRS Journal of Photogrammetry and Remote Sensing*, 60, 315-322.

Francour, P. (1997). Fish assemblages of Posidonia oceanica beds at Port-Cros France, NW Mediterranean: assessment of composition and long-term fluctuations by visual census. *Marine Ecology*, 18 (2), 157-173.

Fyfe, S. K. (2003). Spatial and temporal variation in spectral reflectance: Are seagrass species spectrally distinct? *Limnology and Oceanography*, 48, 464-479.

Gandhi, M. S., Rajamanickam, G. V. (2004). Distribution of certain ecological parameters and foraminiferal distribution in the depositional environment of Palk Strait, east coast of India. *Indian Journal of Marine Sciences*, 33, 287-295.

Hemminga, M., Duarte, C.M. (2000). Seagrass Ecology. Cambridge University Press, United Kingdom.

Hochberg, E. J., Atkinson, M. J. (2000). Spectral discrimination of coral reef benthic communities. *Coral Reefs*, 19, 164-171.

IOCCG, (2000). Remote sensing of Ocean Colour in Coastal, and Other Optically-Complex, Waters. Sathyendranath, S. (Ed.). Reports of the International Ocean-Colour Coordinating Group, nr. 3 IOCCG, Dartmouth, 5-46 pp.

IOCCG, (2010). *Atmospheric Correction for Remotely-Sensed Ocean-Colour Products.* Wang, M. (Ed.). Reports of International Ocean-Color Coordinating Group, nr. 10, IOCCG, Dartmouth, Canada, 78 pp.

Khoi, D. D., Munthali, K. G. (2012). Multispectral Classification of Remote Sensing Data for Geospatial Analysis. *Progress in Geospatial Analysis*, 2012, 13-28.

Kotta, J., Remm, K., Vahtmäe, E., Kutser, T., Orav-Kotta, H. (2014). In-air spectral signatures of the Baltic Sea macrophytes and their statistical separability. *Journal of Applied Remote Sensing*, 8, 083634.

Kutser, T., Dekker, A. G., Skirving, W. (2003). Modeling spectral discrimination of Great Barrier Reef benthic communities by remote sesing instruments. *Limnology and Oceanography*, 48, 497-510.

Kutser, T., Jupp, D. L. B. (2002). Mapping coral reef benthic habitat with a hyperspectral space borne sensor. Proc Ocean Optics XVI, Santa Fe, CD-ROM.

Kutser, T., Metsamaa, L., Vahtmäe, E., Strombeck, N. (2006). On suitability of MODIS 250 m resolution band data for quantitative mapping cyanobacterial blooms. Proceedings of the Estonian Academy of Sciences. *Biology. Ecolody*, 55, 318-328.

Kutser, T., Miller, I., Jupp, D. L. B. (2006a). Maping coral reef benthic substrates using hyperspectral space-borne images and spectral libraries. *Estuarine, Coastal and Shelf Science*, 70, 449-460.

Kutser, T., Vahtmäe, E., Martin, G. (2006b). Assessing suitability of multispectral satellites for mapping benthic macroalgal cover in turbid coastal waters by means of model simulations. *Estuarine, Coastal and Shelf Science,* 67, 521-529.

Laanen, L. M., (2007). Yellow Matters – Improving the remote sensing of Coloured Dissolved Organic Matter in inland freshwaters. Vrije University, Amsterdam, 6-32 pp.

Lalli, M. C., Parsons, R. T., (1994). Biological Oceanography: An Introduction. Pergamon, Vancouver, 45-60 pp.

Lillesand, T., Kiefer, R. (1999). Remote Sensing and Image Interpretation. 4th Edition, John Wiley & Sons Inc., ISBN 0-417-25515-7.

Lyons, M. B., Phinn, S. R., Roelfsema, C. M. (2012). Long term land cover and seagrass mapping using Landsat and object-based image analysis from 1972 to 2010 in the coastal environment of South East Queensland, Australia. *ISPRS Journal of Photogrammetry and Remote Sensing*, 71, 34-46.

Maritorena, S., Morel, A., and Gentili B. (1994). Diffuse reflectance of oceanic shallow waters: Influence of water depth and bottom albedo. *Limnology and Oceanography*, 37, 1689-1703.

Micheli, C., Cupido, R., Lombardi, C., Belmonte, A., Peirano, A. (2012). Changes in Genetic Structure of Posidonia oceanica at Monterosso al Mare (Ligurian Sea) and Its Resilience Over a Decade (1998-2009). *Environmental Management*, 50, pp 598-606.

Miloslavich, P., Díaz, J. M., Klein, E., Alvarado, J. J., Díaz, C., et al. (2010). Marine Biodiversity in the Caribbean: Regional Estimates and Distribution Patterns. *PLoS ONE* 5(8): e11916. DOI:10.1371/journal.pone.0011916.

Minghelli-Roman, A., Chisholm, J. R. M., Marchioretti, M., Jaubert, J. M. (2002). Discrimination of coral reflectance spectra in the Red Sea. *Coral Reefs*, 21, 307-314.

Mishra, D., Narumalani, S., Rundquist, D., Lawson, M. (2006). Benthic Habitat Mapping in Tropical Marine Environments Using QuickBird Multispectral Data. *Photogrammetric Engineering & Remote Sensing*, 72, 1037-1048.

Morel, A., Prieur, L. (1977). Analysis of variations in ocean colour. *Limnology and Oceanography*, 22, 709-722.

Moses, J. W., Gitelson, A. A., Berdnikov, S., Povazhny, V., (2009). Estimation of chlorophyll-a concentration in case II waters using MODIS and MERIS data – successes and challenges. *Environmental Research Letters*, 4, 045005. 8 pp.

Mumby, P. J., Hedley, J. D., Chisholm, J. R. M., Clark, C. D., Ripley, H., Jaubert, J. (2004). The cover of living and dead corals from airborn remote sensing. *Coral Reefs*, 23, 171-183.

Mumby, P. J., Skirving, W., Strong, A. E., Hardy, J. T., LeDrew, E. F., Hochberg, E. J., Stumpf, R. P., David, L. T. (2003). Remote sensing of coral reefs and their physical environment. *Marine Pollution Bulletin*, 48, 219-228.

Mumby, P.J., Clark, C.D., Green, E.P., Edwards, A.J. (1998). Benefits of water column correction and contextual deiting for mapping coral reefs. *International Journal of Remote Sensing*, 19 (1), 203-210.

Ohlendorf, S., Müller, A., Heege, T., Cerdeira-Estrada, S., Kobryn, T. (2011). Bathymetry mapping and sea floor classification using multispectral satellite data and standardized physics-based data processing. *Proc. SPIE* 8175, Remote Sensing of the Ocean, Sea Ice, Coastal Waters, and Large Water Regions 2011, 817503, (October 07, 2011).

Palandro, D. A., Andrefouet, S., Hu, C., Hallock, P., Müller-Karger, F. E., Dustan, P., Callahan, M. K., Kraneburg, C., Beaver, C. R. (2008). Quantification of two decades of shallow-water coral reef habitat decline in the Florida Keys National Marine Sanctuary using Landsat data (1984-2002). *Remote Sensing of Environment*, 112, 3388-3399.

Pasqualini, V., Pergent-Martini, C., Pergent, G., Agreil, M., Skoufas, G., Sourbes, L., Tsirika, A. (2005). Use of SPOT 5 for mapping seagrasses: An application to *Posidonia oceanica. Remote Sensing of Environment*, 94, 39-45.

Philipson, P. (2003). Environmental Applications of Aquatic Remote Sensing. Acta Universitatis Upsaliensis, Uppsala.

Phinn, S.R., Dekker, A.G., Brando, V.E., & Roelfsema, C.M. (2004). Mapping water quality and substrate cover in optically complex coastal and reef waters: an integrated approach. *Marine Pollution Bulletin*, 51, 459-469.

RAMSAR Homepage, http://ramsar.wetlands.org, 13.11.2014.

Ruíz-Rentería, F., Tussenbroek, B. I., Dahlgren, E. J. (1998). CARICOMP – Caribbean coral reef, seagrass and mangrove sites: Puerto Morelos, Quintana Roo, México. Coastal Regions and small island papers. UNESCO, Paris.

Sathyendranath, S. (2000). Remote Sensing of Ocean Colour in Coastal and Other Optically Complex Waters. Reports of the International Ocean-Colour Coordinating Group 3.

Schramm, W., Nienhuis, P.H. (Eds.). (1996). Marine Benthic Vegetation. Recent changes and the Effects of Eutrophication. *Ecological Studies*, Vol. 123. Springer.

Sheinbaum, J., Candela, J., Badan, A., Ochoa, J. (2002). Flow structure and transport in the Yucatan Channel. *Geophysical Research Letters*, 29, 10-1 – 10-4.

Sivalingam, S. (2005). General features and fisheries potential of Palk Bay, Palk Strait and its environs. *Journal of the National Science Foundation of Sri Lanka, 33, 225-232.*

Surrey Satellite Technology Ltd. Homepage, http://www.sstl.co.uk/Press/RapidEye-constellation-launched-successfully, 03.11.2014.

Tulldahl, H. M., Philipson, P., Kautsky, H., Wikström, S. A. (2013). Sea floor classification with satellite data and airborne lidar bathymetry. *Proc. SPIE* 8724, Ocean Sensing and Monitoring V, 87240B (June 3, 2013).

Tyc, G., Tulip, J., Schulten, D., Krischke, M., Oxfort, M. (2005). The RapidEye mission design. *Acta Astronautica*, 56, 213-219.

UNESCO, Water Column Correction Techniques, *Coastal management sourcebooks 3,* Part 2. The Acquisition, Correction and Calibration of Remotely Sensed Data, http://www.unesco.org/csi/pub/source/rs10.htm, 18.03.2015.

UMIACS, Atmospheric correction, 1995. http://www.umiacs.umd.edu/labs/GC/atmo/, 18.03.2015.

Vahtmäe, E. (2005). Mapping benthic algal cover in turbid coastal waters with remote sensing technique. Master Thesis.
http://dspace.utlib.ee/dspace/bitstream/handle/10062/952/vahtmae.pdf?sequence=5, 08.05.2015.

Vahtmäe, E., Kutser, T., Martin, G., Kotta, J. (2006). Feasibility of hyperspectral remote sensing for mapping benthic macroalgal cover in turbid coastal waters - a Baltic Sea case study. *Remote Sensing of Environment*, 101, 342 - 351.

Vahtmäe, E., Kutser, T., Kotta, J., Pärnoja, M. (2011). Detecting patterns and changes in a complex benthic environment of the Baltic Sea. *Journal of Applied Remote Sensing*, 5, 053559.

Vahtmäe, E., Kutser, T. (2007). Mapping Bottom Type and Water Depth in Shallow Coastal Waters with Satellite Remote Sensing. *Jourgnal of Coastal Research*, 50, 185-189.

Vahtmäe, E., Kutser, T. (2013). Classifying the Baltic Sea Shallow Water Habitats Using Image-Based and Spectral Library Methods. *Remote Sensing*, 5, 2451-2474.

Vijayakumar, R., Muthukumar, C., Thajuddin, N., Panneerselvam, A., Saravanamuthu, R. (2007). Studies on the diversity of actinomycetes in the Palk Strait region of Bay of Bengal, India. *Actinomycetologica*, 21, 59-65.

Werdell, P. J., Roesler, C. S. (2003). Remote assessment of benthic substrate composition in shallow waters using multispectral reflectance. *Limnology and Oceanography*, 48, 557-567.

Wikipedia, Aegean Sea, http://en.wikipedia.org/wiki/Aegean_Sea, 16.01.2015.

Wikipedia, La Spezia, http://en.wikipedia.org/wiki/La_Spezia, 15.01.2015.

Wikipedia, Liguria, http://en.wikipedia.org/wiki/Liguria, 15.01.2015.

Wikipedia, MODTRAN, http://en.wikipedia.org/wiki/MODTRAN, 07.03.2015.

Wikipedia, Parco Nazionale delle Cinque Terre, http://en.wikipedia.org/wiki/Parco_Nazionale_delle_Cinque_Terre#cite_note-34, 15.01.2015.

Wikipedia, Thermaic Gulf, http://en.wikipedia.org/wiki/Thermaic_Gulf, 16.01.2015.

Wikipedia, Thessaloniki, http://en.wikipedia.org/wiki/Thessaloniki, 16.01.2015.

Wittlinger, S. K., Zimmerman, R. C. (2000). Hyperspectral remote sensing of subtidal macroalgal assemblages in optically shallow waters. Proc. Ocean Optics XV. CD-ROM.

Non-exclusive licence to reproduce thesis and make thesis public

I,

Laura Lõugas,
(author's name)

1. herewith grant the University of Tartu a free permit (non-exclusive licence) to:

1.1. reproduce, for the purpose of preservation and making available to the public, including for addition to the DSpace digital archives until expiry of the term of validity of the copyright, and

1.2. make available to the public via the web environment of the University of Tartu, including via the DSpace digital archives until expiry of the term of validity of the copyright,

„Using RapidEye high spatial resolution imagery in mapping shallow coastal water benthic habitats",
(title of thesis)

supervised by Tiit Kutser.
(supervisor's name)

2. I am aware of the fact that the author retains these rights.

3. I certify that granting the non-exclusive licence does not infringe the intellectual property rights or rights arising from the Personal Data Protection Act.

Tartu, 15.05.2015